Science of The Total Environment
February 2021, Volume 755, Issue 1, Pages 142355 (17p.)
https://doi.org/10.1016/j.scitotenv.2020.142355
https://archimer.ifremer.fr/doc/00652/76394/

Antagonistic cytoprotective effects of C_{60} fullerene nanoparticles in simultaneous exposure to benzo[a]pyrene in a molluscan animal model.

Moore Michael N. [1, 2, 3, *], Sforzini Susanna [4], Viarengo Aldo [4], Barranger Audrey [1], Aminot Yann [1], Readman James W. [1, 3], Khlobystov Andrei N. [5, 6], Arlt Volker M. [7, 8], Banni Mohamed [9], Jha Awadhesh N. [1]

[1] School of Biological and Marine Sciences, University of Plymouth, Plymouth PL4 8AA, UK
[2] European Centre for Environment & Human Health (ECEHH), University of Exeter Medical School, Knowledge Spa, Royal Cornwall Hospital, Cornwall TR1 3LJ, UK
[3] Plymouth Marine Laboratory, Prospect Place, The Hoe, Plymouth PL1 3HD, UK
[4] Institute for the study of Anthropic impacts and Sustainability in marine environment – IAS, National Research Council – CNR, Via de Marini, 6, 16149 Genova, GE, Italy
[5] School of Chemistry, University of Nottingham, University Park, Nottingham NG7 2RD, UK
[6] Nanoscale and Microscale Research Centre, University of Nottingham, University Park, Nottingham NG7 2RD, UK
[7] Department of Analytical, Environmental and Forensic Sciences, King's College London, London SE1 9NH, UK Department of Analytical, Environmental and Forensic Sciences, King's College London, MRC-PHE Centre for Environmental & Health, London SE1 9NH, UK
[8] Toxicology Department, GAB Consulting GmbH, 69126, Heidelberg, Germany
[9] Laboratory of Biochemistry and Environmental Toxicology, ISA, Chott-Mariem, Sousse, Tunisia

* Corresponding author : Michael N. Moore, email address : mnm@pml.ac.uk

Abstract :

The hypothesis that C60 fullerene nanoparticles (C60) exerts an antagonistic interactive effect on the toxicity of benzo[a]pyrene (BaP) has been supported by this investigation. Mussels were exposed to BaP (5, 50 & 100 µg/L) and C60 (C60 - 1 mg/L) separately and in combination. Both BaP and C60 were shown to co-localise in the secondary lysosomes of the hepatopancreatic digestive cells in the digestive gland where they reduced lysosomal membrane stability (LMS) or increased membrane permeability, while BaP also induced increased lysosomal lipid and lipofuscin, indicative of oxidative cell injury and autophagic dysfunction. Combinations of BaP and C60 showed antagonistic effects for lysosomal stability, mTORC1 (mechanistic target of rapamycin complex 1) inhibition and intralysosomal lipid (5 & 50 µg/L BaP). The biomarker data (i.e., LMS, lysosomal lipidosis and lipofuscin accumulation; lysosomal/cell volume and dephosphorylation of mTORC1) were further analysed using multivariate statistics. Principal component and cluster analysis clearly indicated that BaP on its own was more injurious than in combination with C60. Use of a network model that integrated the biomarker data for the cell pathphysiological processes, indicated that there were significant antagonistic interactions in network complexity (% connectance) at all BaP concentrations for the combined treatments. Loss of lysosomal membrane stability probably causes the release of intralysosomal iron and hydrolases into the cytosol, where iron can generate harmful reactive oxygen species (ROS). It was inferred that this adverse oxidative reaction induced by BaP was

ameliorated in the combination treatments by the ROS scavenging property of intralysosomal C60, thus limiting the injury to the lysosomal membrane; and reducing the oxidative damage in the cytosol and to the nuclear DNA. The ROS scavenging by C60, in combination with enhanced autophagic turnover of damaged cell constituents, appeared to have a cytoprotective effect against the toxic reaction to BaP in the combined treatments.

Graphical abstract

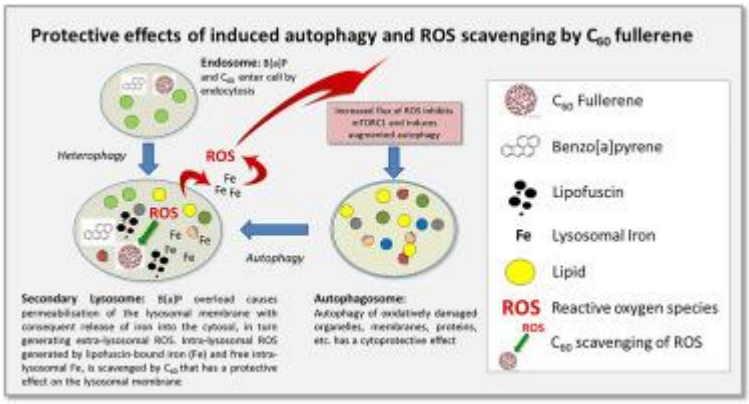

Highlights

► Simultaneous exposure to C_{60} fullerene (C_{60}) and benzo[a]pyrene (BaP) induced antagonistic subcellular interactions in the digestive cells of the digestive gland of the marine blue mussel. ► Both C_{60} and BaP were sequestered in the endolysosomal system where they induced adverse cellular pathological reactions including autophagy; however, those reactions induced by BaP were more severe, with evidence of dysfunctional autophagy. ► Both C_{60} and BaP caused lysosomal overload leading to lysosomal membrane destabilisation (i.e., increased lysosomal membrane permeability), resulting in probable iron release into the cytosol, where it generated harmful reactive oxygen species (ROS) that contributed to oxidative cell injury including DNA damage. ► Network (complexity) modelling of the molecular and subcellular pathology facilitated data interpretation and indicated that autophagy, together with intralysosomal scavenging of ROS by C_{60}, is having a cellular protective effect, compared to exposure to BaP alone.

Keywords : antagonism, autophagy, complexity, lysosomes, C60-nanoparticles, oxidative-injury

Introduction

Manufactured nanomaterials (MNMs) including nanoparticles (NPs), nanotubes and nanofibres are

increasingly used in a burgeoning growth of industrial and domestic applications (Giese et al., 2018). These materials can enter the natural environment via the atmosphere and waterborne waste (Freixa et al., 2018; Giese et al., 2018). There is only limited data available, however, for how these materials will interact with conventional chemical contaminants, such as the ubiquitous contaminant polycyclic aromatic hydrocarbons (PAHs); and whether such interactions can influence the toxicity of either the NPs or the PAHs themselves (Al-Subiai, et al., 2012; Barranger et al., 2019a, b; Canesi et al., 2014; Della Torre et al., 2018; Freixa et al., 2018; González-Soto et al., 2019; Lee et al., 2011; Sforzini et al., 2018, 2020). Previous investigations have indicated that carbon nanomaterials can exert antagonistic interactive effects on the toxicity and ecotoxicity of organic chemical pollutants (Barranger et al., 2019a, b; Freixa et al., 2018).

Accumulating evidence on the toxicity of nanoparticles (NPs) indicates that reactive oxygen species (ROS) mediated oxidative cell injury is a generic reaction (Barranger et al., 2019a, b; D'Agata et al., 2014; Dodd and Jha, 2009; Reeves et al., 2008; Sforzini et al., 2020; Stern et al., 2012; Stone & Donaldson, 2006); although, as yet our understanding of the impact of the products of nanotechnology on animal and ecosystem health is still rather limited (Canesi et al., 2014; D'Agata et al., 2014; Della Torre et al., 2018). Animal cells are evolutionarily pre-adapted to internalise nanomaterials by endocytosis or cell feeding (Stern et al., 2012). Hence, most cellular uptake of NPs will probably occur via this route. Fundamental questions, however, remain unanswered as to the significance of engineered NPs on the health of aquatic organisms, as well as interactions between NPs and conventional chemical pollutants, such as ubiquitous organic xenobiotics (e.g., PAHs and nitrogen and sulphur containing heterocyclics). Of concern also are the higher level consequences for damage to animal health, associated ecological risk and the possible food chain risks for humans.

The lysosomal vacuolar system in the cells of the molluscan digestive gland (hepatopancreas or midgut gland) readily accumulates many harmful environmental contaminants, including metal ions, organic xenobiotics, nano- and micro-plastics and other nanomaterials (Barranger et al., 2019a, b; Jimeno-Romero et al., 2016; Koehler et al., 2008, Lee & Hong, 2020; Moore et al.2004; Sforzini et al., 2018, 2020, Shaw et al., 2019; Von Moos et al., 2012). Lysosomal overload due to sequestration

and accumulation of non-degradable foreign materials (e.g., nanomaterials) and xenobiotic chemicals (e.g., metal ions and organic chemical contaminants) can lead to lysosomal and autophagic dysfunction, involving permeabilisation of the lysosomal membrane and in severe cases release of lysosomal enzymes and cell death (De Duve et al., 1974; Moore et al., 2006, 2007, 2009, Sforzini et al, 2018, 2020; Shaw et al., 2019; Stern et al., 2012). Furthermore, continuous digestion within lysosomes of iron-containing metallo-proteins, from both endocytosed food and autophagy of cell constituents, produces a pool of labile, redox-active, low-molecular-weight iron, which may make these organelles particularly susceptible to oxidative damage (Kurz et al., 2008; Lowe & Moore, 1979; Yu et al., 2003). Oxidant-mediated destabilization of lysosomal membranes with release of iron and hydrolytic enzymes into the cytoplasm can lead to an oxidative and hydrolase-mediated cascade of degradative and injurious events resulting in cell death (Kirchin et al., 1992; Stern et al., 2012; Winston et al., 1991; Yu et al., 2003).

C_{60} fullerene has been reported to induce autophagy in various cells, including molluscan digestive cells using lysosomal membrane destabilisation, lysosomal volume increase and LC3 (microtubule-associated proteins 1A/1B light chain 3B) as the biomarkers (Sforzini et al., 2020; Stern et al., 2012). The autophagic reaction to the nanoparticles is probably mediated by oxidative inhibition (i.e., dephosphorylation) of mTORC1 (mechanistic target of rapamycin complex 1) by an elevated flux of ROS generated as a result of intra-lysosomal iron release into the cytosol, as a result of lysosomal membrane destabilisation (i.e. permeabilisation) as mentioned above (Brunk & Terman, 2002; Sforzini et al., 2020; Stern et al., 2012; Yu et al., 2003).

C_{60} fullerene has the ability to both scavenge and generate (i.e., light-activated) ROS due to its physico-chemical properties (Halenova et al., 2018; Lee et al., 2011). The feature that mediates most of the fullerene's biological and toxic interactions is its particular sensitivity to the covalent attachment of functional groups to the fullerene core, as well as to the physico-chemical changes introduced by solubilisation procedures for the preparation of fullerene nanoparticles (Markovic & Trajkovic, 2008).

Barranger et al. (2019a, b) have previously described antagonistic effects on DNA damage in mussels

for the interactions between benzo[a]pyrene (BaP) and C_{60} fullerene (C_{60}) and multi-walled carbon nanotubes (MWCNTs). Adverse cell pathological effects of BaP and C_{60} individually on DNA damage and sub-cellular injury have also been described from previous investigations (Al-Subiai et al., 2012; Barranger et al., 2019a; González-Soto et al., 2019; Sforzini et al., 2018, 2020).

Consequently, the aim of this investigation was to examine the possible interactive effects of simultaneous exposure to BaP and C_{60} on marine mussels, an ecologically important bio-indicator and ecological foundation species. The hypothesis was tested that C_{60} fullerene exerts a cytoprotective antagonistic interactive effect on the toxicity of BaP (Barranger et al., 2019a, b; Freixa et al., 2018; Lee et al., 2011). Additionally, we also wanted to investigate whether there was any further evidence for either an antagonistic or synergistic ("Trojan Horse") effect between the polycyclic aromatic hydrocarbon BaP and the C_{60} nanoparticles. Chemical analyses of the digestive gland tissue, as well as molecular and sub-cellular biological reactions or biomarkers (viz., DNA damage – Comet assay, LMS, lysosomal lipidosis, lysosomal lipofuscinosis, lysosome/cell – L/C volume as an autophagy biomarker, and phosphorylated mTORC1) were used examine the effects of BaP and C_{60} on tissue uptake, lysosomal function, induced autophagic cellular reactions, and oxidative cell injury. Principal component analysis (PCA) and cluster analysis, together with interactive network or complexity modelling was used to integrate multi-biomarker data into a mechanistic explanatory framework; and to test the predictive capability of a previously developed network complexity model of cellular patho-physiological function for DNA damage (Comet assay) and programmed cell death (PCD) in molluscan digestive cells (Hanni et al., 2017; Barranger et al., 2019a, b; Lowe, 1988; Sforzini et al., 2018). Network complexity and statistical modelling were also deployed in order to facilitate the integration of the biomarker findings and to facilitate their interpretation in a mechanistic context, as was previously implemented with separate BaP and C_{60} fullerene treatments (Sforzini et al., 2018, 2020).

Materials and Methods

Animal Collection and Husbandry

Mussels (*Mytilus galloprovincialis*; 45–50 mm) were collected from the intertidal zone at Trebarwith Strand, Cornwall, UK (50° 38' 40" N, 4° 45' 44" W) in October 2016. This site has previously been

used as a reference location for ecotoxocological studies and is considered relatively clean with a minimum presence of disease (Bignell et al., 2011; Shaw et al., 2011). Following collection, mussels were transported to the laboratory in cool boxes and placed in an aerated tank at a ratio of 1 mussel /L with natural seawater from Plymouth Sound (filtered at 10 µm). Mussels were maintained at 15ºC, fed with micro-algae (*Isochrysis galbana* - Interpret, UK) every 2 days with a 100% water change 2 h post feeding.

Preparation of Stock Solutions

Fullerenes (C_{60})

C_{60} stock solutions were prepared as described by Barranger (2019a). C_{60} was obtained from Sigma Aldrich (Gillingham, UK) and Designer Carbon Materials Ltd. (Oxford, UK), respectively. In order to better replicate the conditions of the experiment during analysis, 2 mussels were maintained in 2 L glass beakers for 24 h with natural seawater from Plymouth Sound (filtered at 10 µm). Subsequently, fullerenes (1 mg) were added to the mussel-exposed seawater (10 mL) and the suspension homogenised by ultrasonication (Langford Sonomatic 375, Bromsgrove, UK, 40 kHz) for 1 h at room temperature. The suspension was allowed to settle for at least 4 h at room temperature prior to analysis of the aggregate size. Dynamic light scattering (DLS) was performed using a Malvern Zetasizer Nano-ZS (Malvern, UK) at room temperature; and the results obtained were the average of 3 measurements (Barranger et al., 2019a). Bright field transmission electron microscopy (TEM) and dark-field scanning transmission electron microscopy (STEM) were performed using a JOEL 2100+ microscope (Welwyn Garden City, UK) operated at 200 keV. Energy dispersive X-ray (EDX) spectra were acquired using an Oxford Instruments INCA X-ray microanalysis system (Oxford, UK) and processed using Aztec software (version 3.1 SP1, Oxford, UK). Samples were prepared by casting several drops of the respective suspensions onto copper grid-mounted lacy carbon films.

The C_{60} concentrations used in this study were based on previous experiments in our laboratory using marine mussels (Al-Subiai et al., 2012; Barranger et al., 2019a; Di et al., 2017; Moore et al., 2009; Sforzini et al., 2020).

Benzo[a]pyrene (BaP)

BaP (≥ 96%, B1760, Sigma Aldrich) was dissolved in dimethyl sulfoxide (DMSO) and aqueous solutions were prepared so that the DMSO concentration in the sea water was 0.001% (Barranger et al., 2019a). The BaP concentrations used in this study were based on previous experiments in our laboratory using marine mussels (Al-Subiai et al., 2012; Di et al., 2011, 2017).

Experimental design, exposure of animals to BaP and C_{60} and sampling

Experimental design has been described in detail by Barranger et al. (2019a). Following depuration, mussels were separated (2 mussels per beaker) into 2 L glass beakers containing 1.8 L of seawater and allowed to acclimate for 48 h. A photoperiod of 12 h light: 12 h dark was maintained throughout the experiment. Seawater was aerated (i.e., aquarium pumps and airstones) and monitored in each of the beakers by measuring salinity with a digital salinity meter (36.15 ± 0.19‰). Mussels (26 mussels with 2 mussels per 2L beaker for each treatment) were exposed for 3 days with no water changes to the solvent control, BaP (5, 50 and 100 µg/L), C_{60} alone (1 mg/L) and a combination of BaP (5, 50 and 100 µg/L) and C_{60} (1 mg/L). Control groups received only DMSO at the same concentrations as used in the other exposure groups (i.e., 0.001% DMSO). After 3-day treatment period, mussel sex was determined by mantle smear and light microscopy. Digestive glands from 10 female animals were rapidly removed, placed on aluminium cryostat chucks, chilled in super-cooled n-hexane and stored at -80°C for cytochemistry and immunocytochemistry (Sforzini et al., 2018). Digestive glands from female mussels were subsequently processed for immunocytochemical and cyotochemical analysis (Sforzini et al., 2018).

Following exposure, digestive gland (DG) tissue was collected from 9 mussels for each treatment for BaP and C_{60} analyses, washed in toluene and pooled (3 mussels per tissue replicate and then extracted with toluene.

Analyses of benzo[a]pyrene and C_{60} fullerene in digestive gland tissue

The analyses of BaP and C_{60} were performed on the toluene extracts. Tissue extracts were analysed

for BaP using an Agilent Technologies (Stockport, UK) 7890A Gas Chromatography (GC) system interfaced with an Agilent 5975 series Mass Selective (MS) detector as described by Banni et al. (2017). The tissue extracts were analysed for C_{60} using ultrahigh performance liquid chromatography coupled with high resolution mass spectrometry following a protocol adapted from Sanchís et al. (2019).

Cytochemical analyses

Frozen digestive gland sections (10 µm) of mussels from each exposure condition were cut using a cryostat microtome (Leica CM3050) and flash-dried by transferring them onto poly-L-lysine-coated microscope slides at room temperature.

Lysosomal membrane stability (LMS)

The determination of LMS in the cells of the digestive gland was performed on cryostat tissue sections following essentially the method described by Moore (1988) and Moore et al. (2008). This cytochemical assay is based on acid labilization characteristics of latent hydrolase β-*N*-acetylhexosaminidase (NAH) using naphthol-AS-BI-N-acetyl-β-D-glucosaminide as a substrate for NAH, and diazonium post-coupled with fast violet B. Slides were observed using an inverted microscope (Zeiss Axiovert 100M) at 400 x magnification, connected to a digital camera (Zeiss AxioCam). The pictures obtained were analysed using an image analysis system (Scion Image) that allowed for the determination of the labilisation period i.e. the incubation time in the acid buffer needed to produce the maximal lysosomal staining.

Lysosomal/cytoplasmic (L/C) volume ratio

The L/C volume ratio of the digestive gland tissue was evaluated following the method described by Moore (1976) and Moore and Clarke (1982). Lysosomes were reacted for the lysosomal enzyme β-*N*-acetylhexosaminidase (NAH) using naphthol-AS-BI-N-acetyl-β-D- glucosaminide as a substrate for NAH as for LMS above. The ratio between cytoplasmic and lysosomal volumes was determined by analysing the images obtained from the slides at 400 × magnification by image analysis as described

above and expressed as a percentage variation with respect to controls.

Lysosomal lipidosis and lipofuscin accumulation

Lysosomal accumulation of triglyceride lipids (neutral lipids) or lipidosis was determined using the Oil Red O method (Moore et al., 2008). Lipofuscin accumulation (lipofuscinosis) in lysosomes was determined *via* the Schmorl assay as previously described (Moore, 1988; Moore et al., 2008). Lipofuscin and lysosomal lipidosis were assessed using image analysis to determine relative absorbance of their respective cytochemical reaction product (Moore 1988; Moore et al., 2008; Sforzini et al., 2020).

Immunocytochemical analyses

Immunofluorescence for BaP, C_{60} fullerene and lysosomal cathepsin D

Frozen digestive gland sections (10 µm) of mussels from each exposure condition were cut using a cryostat microtome (Leica CM3050) and flash-dried by transferring them onto poly-L-lysine-coated microscope slides at room temperature. Sections were then fixed in paraformaldehyde (PFA) solution (4% PFA in phosphate buffer saline-PBS, pH 7.2, 20 min at 20 ± 1 °C).

Immunofluorescent anti-PAHs and anti-C_{60} staining has been described in detail by Sforzini et al. (2018, 2020). To study the possible accumulation of BaP and C_{60} in the lysosomes of the digestive gland cells of exposed mussels, immunofluorescence co-localization of BaP, C_{60} and the lysosomal enzyme cathepsin D was performed following the method described in Sforzini et al. (2018, 2020).

Colocalization of C_{60} and BaP by double immunolabelling with monoclonal antibodies from the same species was performed as described by Eichmüller et al. (1996), with slight modifications. Digestive gland tissue sections were reacted with the anti-fullerene (anti-C_{60}) antibody, as reported above for the single labelling (Sforzini et al., 2020). The anti-PAH antibody (monoclonal mouse, Santa Cruz Biotechnology Inc., 1/100 in PBS containing 1% BSA), used to detect BaP, was coupled *in vitro* to

the secondary antibody (goat polyclonal to mouse Alexa Fluor® 568, 1/50, 1h, 37°C; Sforzini et al., 2014, 2018). Normal mouse serum (0.5%) was then added to saturate excess free anti-mouse binding sites on the secondary antibody (1h at 37°C). Before applying the antibodies-complex solution, sections were incubated with the mouse serum IgG_1 (0.5%, 2% BSA, in PBS, 1h, 20±1°C). Following the immune-reaction with the antibodies-complex (2h, 20±1°C), sections were rinsed in PBS, stained with DAPI and then mounted in Mowiol mounting medium (Cold Spring Harbour Protocols, 2006; http://cshprotocols.cshlp.org/).

Immunofluorescence for anti-phosphorylated-mTORC1

Tissue sections prepared as described above were incubated in a permeabilisation and blocking solution (0.5% Triton X-100, 2% BSA, 0.5% goat serum in PBS, 1 h at 20 ± 1 °C) and then with the primary antibody (anti m-TOR (phospho S2448) antibody, Abcam, 1/100 in PBS containing 1% BSA and 0.05% Triton X-100) overnight at 4 °C in a moist chamber. Sections were then washed three times in PBS (5 min) and the secondary antibody was applied, i.e. polyclonal goat to rabbit (Chromeo) (Abcam) (1/100 in 1% BSA and 0.05% Triton X-100 in PBS) for 1 h at 20 ± 1 °C in the dark. Finally, sections were rinsed in PBS, counterstained with propidium iodide and mounted. Immunocytochemical controls for non-specific fluorescence included sections that were processed in the absence of the primary or secondary antibodies. Slides were viewed under 400 × magnification by an inverted photo-microscope (Zeiss Axiovert 100M connected to a digital camera Zeiss AxioCam MRm) equipped for fluorescence microscopy using FITC, Rhodamine and DAPI emission filters. Images were analysed using an image analysis system (Scion Image) that allowed for the quantification of the mean fluorescence intensity.

Determination of DNA strand breaks using the comet assay

DNA damage (Comet assay) was determined as described in detail by us in earlier publications (Banni et al., 2017; Barranger et al., 2019a,b). Digestive gland tissues were stored on ice prior to processing for the comet assay. After rough chopping, each piece of tissue was added to 1 mL of 1.6 mg/mL dispase II solution (in Hank's buffered saline) pre-warmed to 37ºC. After digesting in the dark

for 30 min, the resulting suspension was coarsely filtered through gauze and spun at 200 *g* to remove any debris. The supernatant was checked for cell viability using trypan blue (0.04%), and only samples with >90% unstained cells were used. A sub-sample of 100 µL of the cell suspension was pelleted at 350 g and 180 µL low melting point agarose added. Two replicate microgels (75 µL) were formed by cover-slipping and allowed to set at 4ºC for a minimum of 15 min. After the cover slips were removed, cells were lysed in 2.5 M NaCl, 100 mM EDTA, 10 mM Tris, 1% N-laurylsarcosine, 1% Triton X-100, and 10% DMSO (adjusted to pH 10 with NaOH) for 1 h at 4ºC in the dark. Slides were then transferred to an electrophoresis chamber containing 1 mM EDTA and 0.3 M NaOH (pH 13). DNA was allowed to unwind in the dark for 20 min, followed by electrophoresis at 1 V/cm (~300 mA) for 20 min in the dark. Gels were preserved with ice cold 100% ethanol and then scored after the addition of 20 µg/mL ethidium bromide using a Leica epifluorescence microscope (Leica Microsystems, Milton Keynes, UK) and Comet 4 image analysis system (Perceptive Instruments, Bury St Edmunds, UK). One hundred nucleoids were assessed per slide; all samples were measured blind. Tail intensity (% tail DNA), defined as the percentage of DNA migrated from the head of the comet into the tail, was used as a measure of DNA damage induced.

Programmed cell death (PCD) determination

Digestive tubule atrophy or breakdown was used as a proxy for PCD and was determined from previously described histopathological and cytochemical investigations of mussel digestive cells by Lowe (1988) and Moore (1988) that enabled the derivation of the relationship between LMS and tubule atrophy (inversely correlated: $R^2 = 0.7745$, $R = -0.8801$, $P \leq 0.001$, $n = 40$).

Univariate statistical analysis

Five replicates per control and experimental treatment concentration were analysed. Each replicate consisted of the digestive gland from one mussel; the mussels were collected from a separate beaker. The non-parametric Mann-Whitney U-test, and the parametric t-test was used to compare the data from treated mussels with those of the controls.

Multivariate statistical analysis

The cellular biomarker data (i.e., LMS, L/C vol., lipid, lipofuscin and phosphorylated mTORC1) for five mussels from each experimental treatment were analysed using non-parametric multivariate analysis software, PRIMER v 6 (PRIMER-E Ltd., University of Auckland, Auckland, New Zealand; Clarke, 1999; Clarke & Warwick, 2001) as previously described by Sforzini et al. (2018, 2020). All data were log transformed [$\log_n(1+x)$] and standardised to the same scale. Correlations between biomarkers were tested using a scatter plot matrix (PRIMER v 6, Draftsman Plot). The multivariate analysis was conducted with and without data for C_{60} at 0.01 and 0.1 mg/L that was reported previously by Sforzini et al. (2020) in addition to C_{60} at 1 mg/L, as was used for the mixtures with BaP treatments. Correlations between the various cellular biomarkers and the first and second principal components (PC 1 & PC 2; C_{60} at 1 mg/L only) were also derived

Finally, in order to map integrated biomarker data onto "health status space" (measured as first principal components – PC 1), PC 1 values were plotted against both the complexity values (system or network complexity - connectance C_v%), and LMS as measures of cellular well-being for each experimental treatment (Sforzini et al., 2018, 2020).

Network modelling

Model description

The generic cell model described by Moore (2010) has been developed from extensive published data in the environmental toxicology and biomedical literature, and the large-scale organisation of metabolic networks (Cuervo, 2004; Di Giulio & Hinton, 2008; Jeong et al., 2000; Juste & Cuervo, 2019; Levine, 2005; Moore, 2020). This cellular interaction network was constructed around the essential processes of feeding, excretion and energy metabolism (Fig 1A). Protein synthesis and degradation, including lysosomal autophagy, and fusion of secondary lysosomes with other secondary lysosomes are also incorporated in the model as are the major protective systems (Livingstone et al., 2000; Moore, 2010; Sforzini et al., 2018). A modified subset of the generic model incorporating

oxidative cell injury was used in this investigation in order to accommodate the available data (Fig. 1B). The directed cellular physiological networks were constructed using *Cytoscape 3.3.0* software (Shannon et al., 2003).

Analysis of cell system complexity

Whole system complexity in the directed cellular physiological network was evaluated using connectedness (Bonchev, 2003). Topological complexity was measured as connectedness or connectance (C_V %) is the ratio between the number of links E in the interaction network and the number of links (edges) in the complete graph having the same number of nodes or vertices (*V*) (Bonchev, 2003). Connectedness relates the number of nodes (vertices) *V* and links or edges (arcs in a directed link) *E* where the connectance percentage ratio, C_V%, of a directed graph (digraph) with *V* nodes or vertices is then:

$$C_V\,\% = [1 / \max (C_V)]\ ||E||\ x\ 100 \quad \textit{(Equation 1)}$$

which reduces to:

$$C_V\,\% = (||E|| / V^2)\ x\ 100 \quad \textit{(Equation 2)}$$

as shown in Equations 1 & 2 for typical digraphs that allow every node to connect to every other node, where ||*E*|| is the nearest integer function of *E* (Davis, 1997). This method uses the sum of the edge weights rather than the edge count and allows for self-loops or arcs (Fig. 1A & B). The network also contained a node for DNA damage although this data was not included in the calculation of connectance. DNA damage (Comet assay) had been determined previously in animals from the same experiment (Barranger et al., 2019a).

Transformed biomarker data were used to attribute proportional weight values to the interactions (edges) between cellular physiological processes (nodes) as previously described (Sforzini et al., 2018; Fig. 1B). The various biomarker values were standardised to a proportion of Control mean values. These values (x) were then used for biomarkers that normally decrease with pathology (i.e., lysosomal membrane stability & mTORC1), while biomarkers that normally increase with pathology (i.e., lysosomal lipid, lysosomal/cell volume ratio & lipofuscin) were further transformed to their

reciprocal value (x^{-1}). All standardised and transformed values were normalised using $\log_{10}$ transformation of x or x^{-1} as appropriate; and then inputted into the model as the weight values for the network interaction strengths (edge or link strength). Finally, the non-parametric Mann-Whitney U-test, and the parametric t-test was applied to the connectance (C_v%) values of the control and experimental treatment groups to test for statistical differences. Network or system complexity was plotted against PC 1, LMS, DNA damage (Comet assay for DNA strand breaks) and predicted PCD.

Analysis of interactions using Interaction Factor (IF)

Analysis of the combined effects of C_{60} and BaP on the biomarkers (i.e., lysosomal membrane stability, mTORC1, lysosomal lipid, lipofuscin & lysosomal/cytoplasmic volume ratio) was performed by calculating the Interaction Factor (IF) in order to test for evidence of additivity, synergism and antagonism as shown in Equations 3-5 (Parrinello et al., 2019a, b; David et al., 2016; Katsifis et al., 1996; Schlesinger et al., 1992; Zhang et al., 2019):

$$IF = (G_{(C60 + BaP)} - C) - [(G_{(C60)} - C) + (G_{(BaP)} - C)] \quad \textit{(Equation 3)}$$

$$= G_{(C60 + BaP)} - G_{(C60)} - G_{(BaP)} + C \quad \textit{(Equation 4)}$$

$$SEM_{(IF)} = \sqrt{(SEM^2_{(C60 + BaP)} + SEM^2_{(C60)} + SEM^2_{(BaP)} + SEM^2_{(C)})} \quad \textit{(Equation 5)}$$

Where IF is the interaction factor: negative IF denotes antagonism, positive IF denotes synergism, and zero IF denotes additivity. G is the mean cell pathological reaction to toxicants (BaP, C_{60} and BaP + C_{60}), C is the mean cellular response under control conditions. For lysosomal membrane stability (LMS) and the phosphorylated mTORC1, the IF value was negatively transformed [-1(IF)] because the experimental treatment generally results in a decrease in the biomarker value compared to the control rather than an increase, which is standard for the IF test. SEM(x) is the standard error of the mean for group X. Results were expressed as IF, and the 95% confidence limits were derived from the combined SEM values.

In order to test the mixture IF values against predicted additive values (assumed to have an IF = 0), the additive mean values (A) were calculated as shown in Equation 6:

$$A = (G_{(C60)} - C) + (G_{(BaP)} - C) \quad \textit{(Equation 6)}$$

The Pythagorean theorem method for combining standard errors was used to derive combined standard errors for the predicted mean additive values (A) of C_{60} and BaP (http://mathbench.org.au/statistical-tests/testing-differences-with-the-t-test/6-combining-sds-for-fun-and-profit/). The standard errors (*SEM*) for the three C_{60} and BaP treatments (predicted additive) were derived using the following Equation 7:

$$SEM_{(add)} = \sqrt{(SEM^2_{(C60)} + SEM^2_{(BaP)} + SEM^2_{(C)})} \quad (Equation\ 7)$$

This enabled the 95% confidence limits to be derived for the predicted additive values. The confidence limits (95% CL/√2) were used to test the predicted additive values having an IF = 0 against the IF values for the mixtures (Buzatto et al., 2015; Lowe et al., 1981).

Results

Analyses of digestive gland for C_{60} and BaP

The results for the chemical analyses of tissues have been previously reported by Barranger et al. (2019a). Both C_{60} fullerene and BaP accumulated in the tissues of the digestive gland (Fig. 2A & B). In our study, we analysed for the first time in a marine bivalve, BaP uptake (at different exposure concentrations) in the digestive gland in the presence of C_{60} fullerene in order to highlight a possible role of contaminant carrier of C_{60}. Comparable BaP tissue concentrations in the presence or absence of C_{60} were observed (Fig. 2A).

Low but quantifiable amounts of C_{60} in digestive gland tissues indicated active uptake, with adsorption on the outside of the tissue ruled out due to external washes with toluene prior to analysis (Fig. 2). High variability in C_{60} concentrations in the digestive gland makes it difficult to detect a difference between treatments in accumulation of C_{60} by mussels.

Biomarker evaluation and cellular localisation of C_{60} fullerene and benzo[a]pyrene

All the different treatments utilised in this study induced adverse cellular reactions (i.e. mTORC1, lysosome/cell volume ratio (L/C volume ratio), lysosomal lipofuscin, lysosomal lipid and DNA damage) in the digestive gland of mussels, without affecting their survival (data not shown) during the time course of the experimental treatments. Representative images for the cellular changes in

mTORC1, lysosome/cell volume ratio (L/C vol.; autophagy biomarker), lipofuscin and lysosomal lipidosis (triglygeride) are shown in Figure 3A-D. Additionally, Figure 4A-D showed that the BaP and C_{60} were both co-localised in the digestive cell secondary lysosomes, using cathepsin-D as an immunocytochemical marker for lysosomes.

As shown in Fig. 5 (A - E), all the biomarkers that were strongly related to the autophagic process (i.e. LMS, phosphorylated mTORC1 and L/C volume ratio) showed a similar trend in mussels exposed to BaP (5, 50, 100 µg/L), C_{60} (1 mg/L), and also in the combined treatments (MIX). In particular, there was a decrease in LMS, and mTORC1 phosphorylation compared to controls. The evaluation of L/C volume ratio showed significant increases in this biomarker in the treated animals, with the exception of the lowest BaP concentration (5 µg/L).

The results for lysosomal lipofuscin content (an oxidative injury biomarker) showed that BaP caused a significant increase of this parameter at all the concentrations tested, with a maximum at 100 µg/L with respect to controls (Fig. 5D). Otherwise, no significant change was observed in C_{60} exposed mussels; while the combined treatments (MIX) showed a similar trend to that of BaP, but for 5 and 50 µg/L BaP with lower values, while the mixture at 100 BaP was not significantly different from the control (Fig. 5D). The evaluation of lysosomal lipid (triglyceride) accumulation (biomarker revealing an alteration of lipid metabolism) showed that in mussels exposed to BaP there was a significant increase of lipid content, with a maximum at 50 µg/L (Fig. 5E). No significant increase was found in C_{60} as well in combined treatment (MIX) of 1.0 mg/L C_{60} and 5 µg/L BaP exposed animals; similar changes to those observed in BaP treatments were induced in animals exposed to the higher MIX concentrations.

Pairwise statistical testing between the BaP and combined (MIX) treatments showed that there were significant decreases ($P \leq 0.05$, Mann-Whitney U-test, t-test) in the combined treatments for LMS (MIX 5, 50 & 100 µg/L BaP) , mTORC1 (MIX 5, 50 & 100 µg/L BaP), lysosomal lipid (MIX 5 & 50 µg/L BaP), lysosomal lipofuscin (MIX 100 µg/L BaP) and network complexity (MIX 5 & 50 µg/L

BaP) compared with the corresponding BaP treatments (Fig. 5A, B, D, E). The autophagy biomarker (L/C volume ratio), however, showed a significant increase ($P \leq 0.05$, Mann-Whitney U-test, t-test) in the combined treatment (MIX 5 µg/L BaP) compared with the corresponding BaP treatment (Fig. 5C).

Multivariate analysis of biomarker reactions

PCA and hierarchical cluster analysis of all the biomarker reactions showed that all experimental treatments compared to the control, had a detrimental effect on the patho-physiology of digestive cells in mussels (ANOSIM, $P \leq 0.01$; Fig. 6). The first principal component (PC 1) represented 52.5% of the variability and is significantly correlated with all five biomarkers (Table 1). However, the second principal component (PC 2), which represented 24.6% of the variance, was strongly correlated with lipofuscin and lysosomal lipid (Table 2), which corresponded to the BaP treatments. Analysis of similarity shows that C_{60} and BaP 100 µg/L were significantly different ($P \leq 0.05$), and that BaP at all three concentrations were significantly different from their corresponding mixtures (ANOSIM, $P \leq 0.01$), and C_{60} and the mixture (C_{60} + BaP 100 µg/L) were significantly different ($P < 0.05$). Overall analysis of similarity showed a highly significant value for dissimilarity (ANOSIM, Global R Statistic: $R = 0.567$, $P \leq 0.001$). Regression analysis (Scatter Plot matrix excluding 0.01 and 0.1 mg/L C_{60}) of the biomarker data indicated that many of the biological parameters were significantly correlated, particularly those directly related to autophagy: - LMS, L/C volume and dephosphorylation of phosphorylated mTORC1 (Fig. 7).

Network modelling biomarker reactions to C_{60} + BaP treatments

Inputting the biomarker data into a directed cellular interaction network (digraph) model (Fig. 1B; Table 2) enabled the determination of the system complexity. Complexity values determined as percentage connectance (C_v%) for the experimental treatments are shown in Figure 5F. There was a significant loss in connectance in all experimental treatments compared with the control ($P \leq 0.005$, Mann-Whitney U-test, t-test). Pairwise statistical testing between the BaP and combined (MIX) treatments showed that there were significant decreases ($P \leq 0.05$, t-test) in the combined treatments for network complexity measured as connectance (MIX 5 & 50 µg/L BaP) compared with the

corresponding BaP treatments (Fig. 5F).

The connectance analysis of these biomarkers data demonstrated that in mussels exposed to all treatments there was a loss of functional complexity (cellular homeostasis), with respect to controls; the maximum loss of connectance was found in animals exposed to 100 µg/L BaP (Fig. 5F).

The determination of node degree indicated that lysosomal function, autophagy and oxidative cell injury were the most highly connected nodes (vertices) with 7 degrees (number of links or edges), making them important patho-physiological hubs (Fig. 1B). In the more comprehensive network shown in Figure 1A, lysosomal function and autophagic function were the most connected nodes, underlining their central role in cellular patho-physiology. System complexity (connectance C_v%) was strongly correlated with the first Principal Component (PC 1, direct), DNA damage (inverse; Comet assay data from Barranger et al., 2019a) and lysosomal stability (direct), as shown in Figure 8A – C (all correlations included data for 0.01 and 0.1 µg/L C_{60} from Sforzini et al, 2020). Complexity was also inversely correlated with estimated or predicted programmed cell death (Fig. 8C; predicted PCD was derived from the previously determined correlation between digestive tubule epithelial atrophy and lysosomal stability shown in the inset of Figure 8C; Lowe, 1988; Lowe et al., 1981; Moore 1988).

Mixture Interactions

The Interaction Factors (IF) for C_{60} fullerene and BaP are shown in Table 3. There was evidence of antagonistic interactions (t-test, significant at the 5% level) between mixtures of C_{60} fullerene and BaP for DNA damage (Comet, MIX 100 µg/L BaP; data from Barranger et al., 2019a), mTORC1 inhibition, lysosomal membrane stability, lysosomal lipofuscin (MIX 100 µg/L BaP), lysosomal lipid (MIX 5 and 50 µg/L BaP), and connectance (Table 3). Furthermore, antagonistic interactions that were just outside the 5% level, but which were significant at the 10% level, were also found for lysosomal/cytoplasmic volume ratio (autophagy) with the MIX 50 and 100 µg/L BaP, and DNA damage with the MIX 50 µg/L BaP. There was no evidence for any synergistic interactions between the test compounds (Table 3).

Discussion

There was no evidence for a synergistic "Trojan Horse" effect when mussels were exposed to mixtures of C_{60} and BaP. In fact, the converse was observed, with strong evidence for a negative (antagonistic) interaction induced by the combined treatments as has been previously described by Freixa et al. (2018) and Barranger et al. (2019a, b); while Lee et al., (2011) have shown that C_{60} was cytoprotective. Canesi et al. (2014) have previously demonstrated both synergistic and antagonistic effects of TiO_2 nanoparticles and TCDD in combination. The findings from these authors indicated an antagonistic effect on lysosomal membrane stability, but that there was a synergistic effect on L/C volume.

Comparable BaP tissue concentrations in the presence or absence of C_{60} were observed (Fig. 2A); and despite the expected strong sorption of BaP on C_{60}, no Trojan horse effect was observed, and C_{60}-sorbed BaP remained bioavailable (Fig. 2A; Barranger et al., 2019a; Linnard et al., 2017). In general, however, high variability for C_{60} tissue concentration, as was observed in the MIX 100 µg/L BaP, may conceal subtle changes.

In a previous study in mussels by Al-Subiai et al. (2012), it has been shown that animals exposed to C_{60} alone exhibited a higher accumulation of C_{60} in the digestive gland compared to the gill. Co-exposure to fluoranthene, however, modified the accumulation of C_{60}, with greater accumulation of C_{60} when animals were exposed to C_{60} alone compared to the combined exposure.

When comparing tissue concentrations for BaP and C_{60}, the bioconcentration observed was much lower for C_{60} compared to BaP. The uptake in the digestive gland of mussels exposed to a similar aqueous concentration of BaP and C_{60} was about 2000 times higher for BaP. However, non-constant concentrations in the aqueous phase, attributed to sorption and/or sedimentation, did not allow the calculation of bioaccumulation factors, which also requires reaching a steady-state in the tissues (Barranger et al., 2019a). The difference between BaP and C_{60} tissue concentration could also be

attributed to different kinetics of uptake that can in future, only be explored through longer exposure periods and regular sampling. Nonetheless, recent work has indicated a continuous increase of C_{60} concentrations in whole mussels over at least three weeks (Sanchís et al., 2018). It is probable that the bioavailability of nanomaterials and their co-contaminants depend on many factors such as their size, shape, surface coating and aggregation state and on the metabolism of the species investigated (Linnard et al., 2017).

C_{60} fullerene and BaP administered separately is known to accumulate in the mussel digestive gland and to be sequestered in the lysosomal compartment (Barranger et al. 2019a; Sforzini et al., 2018, 2020). This investigation has clearly demonstrated that in animals exposed to the combined BaP and C_{60} treatments, the PAH and the nanoparticles accumulated in the lysosomes of the digestive gland cells as confirmed with the localisation of the lysosomal marker protease cathepsin-D (Fig. 4A-D). Lysosomal enlargement in molluscan digestive cells is a feature of autophagy. It also involves lysosomal fusion with a decrease in the number of lysosomes (Choy et al., 2018; Lowe et al., 1981). Autophagy is a highly complex process involving the interactions of many proteins and cell signalling pathways (Zhao & Zhang, 2019). The cell pathology results indicate that autophagy is induced in the digestive cells with all experimental treatments as indicated by reduced lysosomal integrity (LMS) and increased lysosomal/cytoplasmic volume ratio.

C_{60} accumulates in the lysosomal compartment of molluscan hepatopancreatic digestive cells, probably as a result of endocytic uptake as aggregates or individual nanoparticles, or otherwise adsorbed onto food particles by Van der Waal's interactions (Emelyantsev et al., 2019; Di Giosia et al., 2019; Giełdoń et al., 2017; Rashid et al., 1991; Sforzini et al., 2020). C_{60} fullerene has been reported to induce autophagy in various cell types, including molluscan digestive cells using LMS, lysosomal volume increase and LC3 (microtubule-associated proteins 1A/1B light chain 3B) as the biomarkers (Lee et al., 2011; Sforzini et al., 2020; Stern et al., 2012). Accumulation of non-degradable C_{60} in the lysosomal compartment will probably contribute to lysosomal overload and membrane destabilisation with release of iron, and consequent generation of ROS in the cytosol

(Sforzini et al., 2020; Stern et al., 2012; Yu et al., 2003). This increased flux of ROS will probably be the major trigger for an augmented autophagic reaction to the nanoparticles by oxidative inhibition (dephosphorylation) of mTORC1 (mechanistic target of rapamycin complex 1; Cuervo, 2004; Moore, 2020). Autophagy induced by C_{60} appears to be cytoprotective. Although there was some evidence of ROS mediated oxidative damage, such as increased lysosomal fragility, this response was limited and there was no evidence for serious oxidative stress, as would be characterised by the lack of lipofuscin accumulation in the lysosomal compartment (Lee et al., 2011; Moore et al., 2020; Sforzini et al., 2018, 2020; Shaw et al., 2019).

Accumulation of lysosomal lipofuscin is an effective indicator of oxidative cell injury (Moore et al., 2006; Sforzini et al., 2018). As mentioned above, the C_{60} treatment did not appear to cause significant oxidative cell injury, as there was no increase in lipofuscin (Sforzini et al., 2020). However, oxidative cell injury was observed in the three BaP treatments probably caused by increased generation of ROS, accompanied by increased lysosomal lipofuscin and lipid, and reduced lysosomal membrane stability (Fig. 2B, C & D; Fig. 4A, D & E; Jaishy & Abel, 2016; Seranova et al., 2017; Sforzini et al., 2018, 2020). Lipofuscin was elevated in the MIX 5 and 50 µg/L BaP treatments. The trend was, however, lower than in the BaP-treated animals and significantly lower at the MIX 100 µg/L BaP ($P \leq 0.05$, Mann-Whitney U-test). It was also significantly antagonistic in the MIX 100 µg/L BaP treatment (Table 3). However, the PCA indicated that this induced autophagy could be differentiated into probable augmented functional autophagy, and augmented but tending towards dysfunctional autophagy (Fig. 6; Moore et al., 2020; Shaw et al., 2019). All of the cellular biomarkers correlated with PC 1 (Table 1), whereas PC 2 was strongly correlated with lysosomal lipofuscin and lysosomal lipid content (Table 1), both of which are indicative of dysfunctional autophagy, with inhibition of lysosomal degradative enzymes (Jaishy & Abel, 2016; Shaw et al., 2019). The BaP treated mussels contributed to the alignment with the second principal component (PC 2), while the C_{60} and mixture treatments aligned with the first principal component (PC 1) as indicated in Figure 8A. The PCA also indicates that there is probably an antagonistic interaction in the mixtures (Fig. 6).

Excessive lipofuscin accumulation in lysosomes is also harmful in its own right, due to the production of ROS by lipofuscin-bound iron (Brunk & Terman, 2002). Consequently, much of the observed DNA damage will probably have resulted from oxidative injury caused by ROS generated by the release of reactive iron from within the lysosomal compartment, as well as increased ROS produced by iron bound to lysosomal lipofuscin (Barranger et al., 2019a; Brunk & Terman, 2002; Sforzini et al., 2018, 2020; Zanger et al., 2004). There was no evidence for the formation of DNA adducts as a result of interactions with oxidative metabolites of BaP (Barranger et al., 2019a).

Dysfunctional autophagy characterised by swollen lipid-rich lysosomes (triglyceride lipidosis) can also contribute to an increased level of programmed cell death (Fig. 3D; Cuervo, 2004; Lowe, 1988; Sforzini et al., 2018). This was further reflected as reduced lysosomal membrane stability and associated indications of dysfunctional autophagy was strongly linked with digestive tubule atrophy as a result of programmed cell death (PCD) based on re-analysis of previously published findings (Lowe, 1988; Moore, 1988).

PCA and cluster analysis, however, does not integrate the various biomarkers in a functionally meaningful way. It is only the first stage in developing numerical and network models for environmental impact on the health of sentinel animals such as mussels and earthworms (Moore, 2010; Sforzini et al., 2015, 2016, 2020). In order to encapsulate the cellular physiological processes, it is necessary to interconnect the biomarker data within a logical mechanistic framework. Previous studies have used a network model of the physiological and pathological processes known to occur in the digestive cells (Moore et al., 2015; Sforzini et al., 2018). Complexity is a measure of the interconnectedness of the network and can be used as an indicator of homeostasis (Lewis et al., 1992; Moore, 2010; Moore et al., 2015; Sedivy, 1999). Complexity of the whole system increases when sub-systems, such as detoxication and anti-oxidant protective processes, augmented autophagy, protein degradation and induction of stress proteins, are up-regulated and start to interact significantly as part of a response to low-level stress (i.e., biphasic or hormetic response; Moore, 2010, 2020; Moore et al., 2015, 2020). However, with increasing severity of stress, cell injury and higher-level functional

impairment lead to physiological dysfunction, pathology and breakdown of the whole interaction network with consequent loss of complexity (Moore, 2010). Consequently, inputting the biomarker data from the C_{60} + BaP exposure experiment into a directed cell patho-physiological network model showed that there was a statistically significant reduction in system complexity with increasing tissue BaP (chemical data from Barranger et al., 2019a; Sforzini et al., 2018), in both the presence and absence of C_{60}. This indicated decreased homeostasis and health status (Fig. 5F; Barranger et al., 2019a). The model demonstrates that autophagy is an important highly connected hub in the cellular physiology network of the system being tested. This lends support to the overall hypothesis, namely, that autophagy, lysosomal function, oxidative cell injury and mTOR signalling are intrinsically interlinked in physiological responses and patho-physiological reactions to stress (Fig. 1A). The strong correlations between network complexity versus the first principal component, DNA damage, lysosomal membrane stability and estimated programmed cell death further support the use of system complexity as a measure of cellular homeostasis, and the capability to extrapolate to higher level effects (e.g., predicted PCD; Fig. 8A-D).

The network approach supports the hypothesis that stress leading to pathology results in a loss of system complexity as previously described by Moore (2010). Consequently, cellular networks can be used to integrate information from biomarker data; and to direct the selection of biomarkers and design of experiments, in order to develop suites of tests that will demonstrate which links are active or inactive, and to what degree. This provides mathematical formalism for an objective evaluation of health status based on measurement of various biomarkers for potential use in risk assessment (Moore, 2010, Moore et al., 2015; Sforzini et al., 2018). The strong correlation between system complexity and DNA damage indicates that this type of modelling has potential for predicting cellular pathological endpoints (Barranger et al., 2019a; Canova et al., 1998; Fig. 1A). DNA damage was included in the network model as an endpoint, although the values from the Comet assays were not required for the calculation of connectance as DNA damage was an endpoint with uni-directional links from oxidative stress and autophagy (Fig. 1B, Table 2).

Pairwise testing of the BaP and combined (MIX) treatments showed that there were significant decreases at all concentrations of BaP for LMS and mTORC1, while the other biomarkers showed significant decreases at particular concentrations of BaP, but not all (Fig. 5). Network or system complexity was also decreased in the two lower BaP concentration combined treatments (MIX 5 and 50 µg/L BaP; Fig. 5). The autophagy biomarker (L/C volume ratio), however, was increased in the lowest combined treatment (MIX 5 µg/L BaP; Fig. 5). Interaction factors (Ifs) generally indicated that cell injury was statistically additive at MIX 5 and 50 µg/L BaP, but was antagonistic at MIX 100 µg/L BaP, based on the lipofuscin levels (Table 3). There appeared, however, to be an intracellular limiting effect on oxidative cell injury in some of the test mixture treatments, as exemplified by the antagonistic interactions for DNA damage (MIX 100 µg/L BaP), phosphorylated mTORC1 kinase, LMS, lysosomal lipofuscin (MIX 100 µg/L BaP) and lysosomal lipid accumulation (MIX 100 µg/L BaP; Table 3). The additional evidence from the PCA and network analyses support the interpretation that this amelioration in cell injury in the mixtures may be caused either by a reduction in ROS generation, or else by more effective scavenging of ROS by C_{60}, when C_{60} and BaP are present together in close association, as previously described (Della Torre et al. 2018; Di et al. 2017). C_{60} fullerenes are both cytoprotective scavengers and generators of ROS (Barranger et al., 2019a; Lee et al., 2011; Rondags et al., 2017; Sforzini et al., 2020); and when C_{60} fullerene and BaP are closely associated, or bound together within the overloaded lysosomal compartment of the mussel digestive cells, the ROS scavenging ability of C_{60} is probably a significant factor (Fig. 9A-C; Barranger et al., 2019; Stern et al., 2012).

Uptake of both BaP and C_{60} is probably mediated by endocytosis, associated with food proteins or else bound to cell surface proteins mediated by Van der Waals interaction (Emelyantsev et al., 2019; Di Giosia et al., 2019; Giełdoń et al., 2017; González-Soto et al., 2019; Moore et al., 2004; Oh & Park, 2014; Rashid et al., 1991; Sayes et al., 2004). BaP may also enter the digestive cells through a combination of direct transfer (Plant et al., 1985); as well as through endocytosis in bound form with C_{60} and food proteins and lipids (Barranger et al., 2019a; Sforzini et al., 2018). However, mTORC1 is inhibited by ROS and oxidative damage, which will probably limit endocytic uptake of particle

associated BaP and C_{60} + bound BaP (Zhao et al., 2017). Inhibition of mTORC1 will also trigger decreased LMS, as well as increased autophagy and programmed cell death (i.e., PCD type 1 – apoptosis, PCD type 2 – autophagic cell death and PCD type 3 – necrotic cell death; Cuervo, 2004; Seo et al., 2018; Wang et al., 2018). Previous studies have shown that PAHs such as fluoranthene, 3-methylcholanthrene and BaP accumulate in the lysosomal compartment; where they destabilise the lysosomal membrane releasing lysosomal iron, hence, inducing oxidative cell injury and dysfunctional autophagy in the hepatopancreatic digestive cells (Kurz et al., 2008; Moore et al., 2006, 2007; Sforzini et al., 2018; Shaw et al., 2019; Stern et al., 2012). Autophagy and lysosomal function can become dysfunctional due to excessive lipid and lipofuscin accumulation (Brunk & Terman, 2002; Jaishy & Abel, 2016; Kurz et al., 2008).

There was strong evidence for interactions in the biomarker and connectance data for the three combinations of BaP and C_{60} fullerene (Barranger et al., 2019a, b; David et al., 2016; Katsifis et al., 1996; Schlesinger et al., 1992; Zhang et al., 2019). The antagonistic interactions reported here can be interpreted as a cytoprotective effect against the cytotoxicity of BaP being exerted by C_{60} scavenging of ROS generated by BaP overload within the lysosomal compartment (Barranger et al., 2019a, b; David et al., 2016; Katsifis et al., 1996; Lee et al., 2011; Schlesinger et al., 1992; Sforzini et al., 2018; Stern et al., 2012; Zhang et al., 2019). Augmented autophagy induced by oxidative inhibition of mTORC1 will also have contributed to the cytoprotective effect of C_{60} (Lee et al., 2011; Moore, 2020; Moore et al., 2020; Sforzini et al., 2020). However, C_{60} does also exert cytotoxicity in its own right, so the cytoprotective properties appear to be superimposed on the toxicity of BaP when the two compounds are used in combination (Fig. 9A-C). C_{60} is known to have cytoprotective properties as well as being a generator of ROS (Rondags et al., 2017; Zhang et al., 2019). Since ROS generation by C_{60} is induced by visible light, it is considered unlikely that C_{60} is producing significant ROS within the lysosomal-vacuolar system of the digestive cells: rather the sequestration of non-degradable C_{60} in the lysosomes will cause limited release of intra-lysosomal iron that will in turn, generate ROS and inhibit mTORC1, thus triggering protective augmented autophagy (Kirchin et al., 1992; Moore, 2020; Moore et al., 2020; Sforzini et al., 2020; Stern et al., 2012; Winston et al., 1991; Zhao & Zhang,

2019). The findings of Barranger et al. (2019a) and the current data support the cytoprotective interpretation of internalised C_{60} nanoparticles (Fig. 8C). In fact, the chemical analytical data reported by Barranger et al. (2019a) indicated that the internalisation of C_{60} was considerably enhanced when mussels were treated at the highest experimental concentration of BaP (100 µg/L), in comparison with the lower treatment concentrations (Fig 2B). The explanation for this is not readily apparent, however, the chemical data for C_{60} + BaP (100 µg/L) had high variability (Fig. 2B; Barranger et al., 2019a).

The digestive gland, liver analogue, is probably the most important organ for the health of the mussel. Damage to this organ, as described in this investigation, has the potential for serious higher level adverse impacts on the functionality of the whole animal. This cell injury, in turn, will have potential eco-pathological consequences for the mussel population and functional ecology of the ecological assemblages that are dependent on mussels as ecological foundation species (Moore et al., 2013).

The network modelling has facilitated the further refinement of an integrated conceptual mechanistic framework described by Sforzini et al. (2018) that encapsulates the interrelated patho-physiological processes involved in the cellular reactions to C_{60} and BaP. These processes have been described diagrammatically in Figure 10, and in a network format in Figure 1A. Although most of these processes are considered to be evolutionarily highly conserved, some have not yet been confirmed to occur in molluscs (i.e., mTORC1 links with the regulation of endocytosis and MDR/Pgp40 multi-drug resistance transporter) (Bova, 2012; Flinn & Backer, 2010; Grahammer et al., 2016; Jiang & Liu, 2008; Wang et al., 2018). Physiological augmented autophagy is activated by the inhibition of mTORC1, along with reduced lysosomal membrane permeability or LMS. This can be triggered by a number of environmental factors, including low nutrient concentration and oxidative stress (Moore et al., 2007; Seranova et al., 2017; Zhao et al., 2017).

As previously described, hypothesised functional links between endocytic uptake of C_{60} and BaP with natural particles, transfer to the lysosomal system, where accumulation will be further facilitated by the presence of P-glycoprotein (MDR-Pgp40) in the lysosomal membrane (Minier & Moore, 1996a, b; Yang et al., 2002). The demonstrated accumulation of C_{60} fullerene, BaP and lipid in the lysosomal

compartment will probably result in ROS generation and formation of lipofuscin or stress/age pigment (Brunk & Terman, 2002; Moore et al., 2006; Sforzini et al., 2018). However, C_{60} fullerene is indicated to have a cytoprotective role in scavenging ROS generated by BaP in the mixture treatments as shown diagrammatically in Figure 6. mTORC1 inhibition by ROS is probably a further contributory factor to cytoprotection in the C_{60} + BaP mixtures as this inhibition will result in augmented functional autophagy, whereas BaP on its own will shift the balance towards dysfunctional autophagy (Fig. 9A-C; Moore et al., 2020; Sforzini et al., 2018, 2020; Shaw et al., 2019).

The network model shown in Figure 1A and B indicates that lysosomal function and autophagy are both highly connected nodes, and as such form important hubs in the cellular physiology of the digestive cells. Consequently, physiological hub dysfunction as a result of xenobiotic and NP overload and the associated oxidative attack, is indicative of the importance of both these linked modular cellular systems to the normal functioning of the digestive cells as well as in the cell's response to stress (Stern et al., 2012). The relative homogeneity of the responses of network complexity responses (connectance) to the experimental treatments as shown in Figure 5F, indicates that the animals are effectively compensating for the environmental insults and have established a new steady state (Moore, 2010; Stelling et al., 2004). An explanation for this may be that even if individual nodes (vertices) are compromised, the system or network can compensate by bypassing or modifying the interaction strengths for the damaged node, and utilise alternative processes and pathways to minimise network disruption and the degree of cell injury (Fig. 1A; Stelling et al., 2004). Stelling et al. (2004) has previously demonstrated that functional cellular networks are highly robust when perturbed by environmental and other stressors, and will establish a new physiological state unless a key hub (highly connected node) or several hubs is compromised.

In the future, the individual nodes in the network representing cellular processes can potentially be further modelled at lower levels of biological organisation by inputting transcriptomic and proteomic data as has been initiated by Banni et al. (2017) and Barranger et al. (2019a,b). This capability will probably be enhanced by future improvements in our knowledge of protein-protein interactions (interactome); as well as how effectively gene expression correlates with the proteome and is represented by functional interacting proteins. However, at present the pathways that regulate the

kinetics of transcriptional and translational activity and post-translational modification of proteins during cell maturation are not well defined (Hoogendijk et al., 2019). In addition, the often low correlation between the transcriptome and the proteome supports the view that post-transcriptional processes play a major role in the adaptation to altered physiological conditions (Bathke et al., 2019).

Conclusions

The hypothesis that C_{60} fullerene exerts an antagonistic interactive effect on the toxicity of benzo[a]pyrene has been supported by this investigation. BaP and C_{60} were shown to co-localise in the secondary lysosomes of the hepatopancreatic digestive cells in the digestive gland. Combinations of BaP and C_{60} showed antagonistic effects for lysosomal membrane stability, mTORC1 inhibition, lysosomal lipofuscin and lysosomal lipid (MIX 5 & 50 µg/L BaP). Previous reports based on data from the same investigation have indicated an antagonistic interaction for DNA damage. The biomarker data analysed using multivariate statistics: principal component and cluster analysis clearly showed that BaP on its own was more injurious than when in combination with C_{60}. When the biomarker data were incorporated in an interactive network model describing the main cell pathology processes, the integrated outputs (connectance – C_v%) for the system complexity (i.e., essentially a measure of system integrity or homeostasis) showed that there was a significant antagonistic interaction at all BaP concentrations for the combined treatments. It is inferred that oxidative cell injury reactions induced by BaP are ameliorated in the combination treatments by the ROS scavenging property of intralysosomal C_{60}. This limits the injury to the lysosomal membrane, reducing the oxidative damage in the cytosol and to the DNA. The ROS scavenging by C_{60} in combination with enhanced autophagic turnover of damaged cell constituents appears to have a cytoprotective effect against the toxic reaction to BaP in the combined treatments

Furthermore, the loss of cellular physiological complexity in the hepatopancreatic digestive cells, has a potential predictive capability, since complexity correlated inversely with DNA damage. It also inversely correlated with the degree of predicted PCD caused by the experimental treatments based on the inverse correlation between lysosomal membrane stability and digestive tubule atrophy. The network model deployed in this investigation and a previous study of the effects of BaP is a subset of a larger network model incorporating other processes that were not included in this study, but that are

known to be involved in the patho-physiology and induced molecular toxicology of mussels. It is suggested that the inclusion of a larger group of molecular and cellular biomarkers in future studies, as indicated in this larger network, will give a more comprehensive picture of the cellular dysfunctionality caused by environmental nanomaterials and toxic xenobiotics in the molluscan digestive gland (hepatopancreas) following environmental insult.

Acknowledgements

This study was supported financially by the Natural Environment Research Council (NERC), UK (Grant No.NE/L006782/1; PI: ANJ). There are no conflicts of interest.

References

Al-Subiai, S.N., Arlt, V.M., Frickers, P.E., Readman, J.W., Stolpe, B., Lead, J.R., Moody, A.J., Jha, A.N., 2012. Merging nano-genotoxicology with eco-genotoxicology: An integrated approach to determine interactive genotoxic and sub-lethal toxic effects of C_{60} fullerenes and fluoranthene in marine mussels, *Mytilus* sp. Mutat. Res. Genet. Toxicol. Environ. Mutagen., 745, 92–103.

Banni, M., Sforzini, S., Arlt, V.M., Barranger, A., Dallas, L.J., Oliveri, C., Aminot, Y., Pacchioni, B., Millino, C., Lanfranchi, G., Readman, J.W., Moore, M.N., Viarengo, A., Jha, A.N., 2017. Assessing the impact of Benzo[a]pyrene on Marine Mussels: Application of a novel targeted low density microarray complementing classical biomarker responses. PLoS One 12(6):e0178460. doi: 10.1371/journal.pone.0178460.

Barranger, A., Langan, L.M., Sharma, V., Rance, G.A., Aminot, Y., Weston, N.J., Akcha, F., Moore, M.N., Arlt, V.M., Khlobystov, A.N., Readman, J.W., Jha, A.N., 2019a. Antagonistic interactions between benzo[a]pyrene and fullerene (C_{60}) in toxicological response of marine mussels. Nanomaterials (Basel) 8;9(7). pii: E987. doi: 10.3390/nano9070987.

Barranger, A., Rance, G.A., Aminot, Y., Dallas, L.J., Sforzini, S, Weston, N.J., Lodge, R.W., Banni, M., Arlt, V.M., Moore, M.N., Readman, J.W., Viarengo, A., Khlobystov, A.N., Jha, A.N., 2019b. An integrated approach to determine interactive genotoxic and global gene expression effects of multiwalled carbon nanotubes (MWCNTs) and benzo[a]pyrene (BaP) on marine mussels: evidence of reverse 'Trojan Horse' effects. Nanotoxicology 13, 1324-1343.

Bathke, J., Konzer, A., Remes, B., McIntosh, M., Klug, G., 2019. Comparative analyses of the

variation of the transcriptome and proteome of *Rhodobacter sphaeroides* throughout growth. BMC Genomics 20, 358; https://doi.org/10.1186/s12864-019-5749-3.

Bignell, J.P., Stentiford, G.D., Taylor, N.G., Lyons, B.P., 2011. Histopathology of mussels (*Mytilus* sp.) from the Tamar estuary, UK. Mar. Environ. Res., 72(1-2), 25-32.

Bonchev, D., 2003. Complexity of protein-protein interaction networks, complexes, and pathways. In: Handbook of proteomic methods (Ed. P.M. Conn) pp. 451-462. Humana Press, Totowa, New Jersey.

Boya, P., 2012. Lysosomal function and dysfunction: mechanism and disease. Antiox. Redox Signaling 17, 766-774.

Brunk, U.T., Terman, A., 2002. Lipofuscin: mechanisms of age-related accumulation and influence on cell function. Free Rad. Biol. Med. 33, 11-619.

Buckland-Nicks, J., Hodgson, A.N., 2005. Paraspermatogenesis of cerithioidean snails: retention of an acrosome and nuclear remnant. J. Morphology 264, 314-326.

Buzatto, B.A., Kotiaho, J.S., Tomkins, J.L., Simmons, L.W., 2015. Intralocus tactical conflict: genetic correlations between fighters and sneakers of the dung beetle *Onthophagus taurus*. J. Evolut. Biol., 28, 730-738.

Canesi, L., Frenzilli, G., Balbi, T., Bernardeschi, M., Ciacci, C., Corsolini, S., Della Torre, C., Fabbri, R., Faleri, C., Focardi, S., Guidi, P., Kočan, A., Marcomini, A., Mariottini, M., Nigro, M., Pozo-Gallardo, K., Rocco, L., Scarcelli, V., Smerilli, A., Corsi, I., 2014. Interactive effects of n-TiO2 and 2,3',8-TCDD on the marine bivalve *Mytilus galloprovincialis*. Aquatic Toxicol., 153, 53-65.

Canova, S., Degan, P., Peters, L.D., Livingstone, D.R., Voltan, R., Venier, P., 1998. Tissue dose, DNA adducts, oxidative DNA damage and CYP1A-immunopositive proteins in mussels exposed to waterborne benzo[a]pyrene. Mutation Res/Fundamental and Molecular Mechanisms of Mutagenesis 399, 17-30.

Chen, L., Xu, B., Liu, L., Luo, Y., Yin, J., Zhou, H., Chen, W., Shen, T., Han, X., Huang, S., 2010. Hydrogen peroxide inhibits mTOR signaling by activation of AMPKa leading to apoptosis of neuronal cells. Lab. Invest. 90, 762-773.

Choy, C.H., Saffi, G., Gray, M.A., Wallace, C., Dayam, R.M., Ou, Z.-Y.A., Lenk, G., Puertollano, R., Watkins, S.C., Botelho, R.J., 2018. Lysosome enlargement during inhibition of the lipid kinase PIKfyve proceeds through lysosome coalescence. J. Cell Sci., 131(10), jcs213587. doi:10.1242/jcs.213587.

Clarke, K.R., 1999. Non-metric multivariate analysis in community-level ecotoxicology. Environ. Toxicol. Chem. 18, 117-127.

Clarke, K.R., Warwick, R.M., 2001. Change in marine communities: an approach to statistical analysis and interpretation. PRIMER-e, Plymouth, UK.

Cuervo, A.M. (2004) Autophagy: in sickness and in health. TRENDS Cell Biol., 14, 70-77.

David, R., Ebbels, T., Gooderham, N., 2016. Synergistic and antagonistic mutation responses of human MCL-5 cells to mixtures of benzo[a]pyrene and 2-amino-1-methyl-6-phenylimidazo[4,5-528 b]pyridine: dose-related variation in the joint effects of common dietary carcinogens. Environ. Health Perspect., 124, 83-96.

Davis, M.W., 1997. Complexity formalisms, order and disorder in the structure of art. In: Evolutionary Programming VI, Lecture Notes in Computer Science (Editors: Angeline PJ, Reynolds, McDonnell JR, Eberhart R), Vol. 1213, Springer International Publishing AG, Switzerland. pp 1-12.

D'Agata, A., Fasulo, S., Dallas, P.J., Fisher, A.S., Maisano, M., Readman, J.W., Jha, A.N., 2014. Enhanced toxicity of 'bulk' titanium dioxide compared to 'fresh' and 'aged' nano-TiO_2 in marine mussels (*Mytilus galloprovincialis*). Nanotoxicology, 8, 549-558.

De Duve, C., De Barsy, T, Poole, B., Trouet, A., Tulkens, P., Van Hoof, F., 1974. Commentary. Lysosomotropic agents. Biochem. Pharmacol., 23, 2495–2531.

Della Torre, C., Maggioni, D., Ghilardi, A., Parolini, M., Santo, N., Landi, C., Madaschi, L., Magni, S., Tasselli, S., Ascagni, M., Bini, L., La Porta, C., Del Giacco, L., Binelli, A., 2018. The interactions of fullerene C_{60} and benzo[α]pyrene influence their bioavailability and toxicity to zebrafish embryos. Environ. Pollut., 241, 999-1008.

Di Giosia, M., Valle, F., Cantelli, A., Bottoni, A., Zerbetto, F., Calvaresi, M., 2018. C_{60} bioconjugation with proteins: towards a palette of carriers for all pH ranges. Materials 2018, 11,

691; doi:10.3390/ma11050691.

Di Giulio, R.T., Hinton, D.E., Editors, 2008. The toxicology of fishes. Taylor and Francis, London, New York, Singapore, Melbourne, 1071 p.

Di, Y., Aminot, Y., Schroeder, D.C., Readman, J.W., Jha, A.N., 2017. Integrated biological responses and tissue-specific expression of *p53* and *ras* genes in marine mussels following exposure to benzo(α)pyrene and C_{60} fullerenes, either alone or in combination. Mutagenesis 32, 77-90.

Di, Y., Schroeder, D.C., Highfield, A., Readman, J.W., Jha, A.N., 2011. Tissue specific expression of p^{53} and *ras* genes in response to the environmental genotoxicants Benzo(a)pyrene in marine mussels. Environmental Science and Technology 45, 8974-8981.

Dodd, N.J.F., Jha, A.N., 2009. Titanium dioxide induced cell damage: A proposed role of the carbonyl radical. Mutation Research (*Fundamental and Molecular Mechanisms of Mutagenesis*), 660, 79-82.

Eichmüller, S., Stevenson, P. A., Paus, R., 1996. A new method for double immunolabelling with primary antibodies from identical species. J. Immunol. Methods, 190, 255-265.

Emelyantsev, S., Prazdnova, E., Chistyakov, V., Alperovich, I., 2019. Biological effects of C_{60} fullerene revealed with bacterial biosensor—toxic or rather antioxidant? Biosensors, 9, 81; doi:10.3390/bios9020081.

Flinn, R.J., Backer, J.M., 2010. mTORC1 signals from late endosomes: taking a TOR of the endocytic system. Cell Cycle, 9, 1869-1870.

Freixa, A., Acuna, V., Sanchis, J., Farre, M., Barcelo, D., Sabater, S., 2018. Ecotoxicological effects of carbonbased nanomaterials in aquatic organisms. Sci. Total Environ., 619-620, 328-337.

Giełdoń, A., Witt, M.M., Gajewicz, A., Puzyn, T., 2017. Rapid insight into C_{60} influence on biological functions of proteins. Structural Chemistry, 28:1775–1788.

Giese, B., Klaessig, F., Park, B., Kaegi, R., Steinfeldt, M., Wigger, H., Von Gleich, A., Gottschalk, F., 2018. Risks, release and concentrations of engineered nanomaterials in the environment. Scientific Reports, 8(1), 1565. doi:10.1038/s41598-018-19275-4.

González-Soto, N., Hatfield, J., Katsumiti, A., Duroudier, N., Lacave, J.M., Bilbao, E., Orbea, A., Navarro, E., Cajaraville, M.P., 2019. Impacts of dietary exposure to different sized polystyrene

microplastics alone and with sorbed benzo[a]pyrene on biomarkers and whole organism responses in mussels *Mytilus galloprovincialis*. Sci. Tot. Environ., 684, 548-566.

Grahammer, F., Ramakrishnan, S. K., Rinschen, M. M., Larionov, A. A., Syed, M., Khatib, H., Roerden, M., Sass, J. O., Helmstaedter, M., Osenberg, D., Kühne, L., Kretz, O., Wanner, N., Jouret, F., Benzing, T., Artunc, F., Huber, T. B., Theilig, F. (2016). mTOR regulates endocytosis and nutrient transport in proximal tubular cells. J. Am. Soc. Nephrol., 28, 230-241.

Halenova, T., Raksha, N., Vovk, T., Savchuk,O., Ostapchenko, L, Prylutskyy,Y., Kyzyma, O., Ritter, U., Scharff, P., 2018. Effect of C_{60} fullerene nanoparticles on the diet-induced obesity in rats. Int J Obes 42, 1987–1998.

Hoogendijk, A.J., Pourfarzad, F., Aarts, C.E.M., Tool, A.T.J., Kiemstra, I.H., Grassi, L., Frontini, M., Meijer, A.B., van den Biggelaar, M., Kuijpers, T.W., 2019. Dynamic transcriptome-proteome correlation networks reveal human myeloid differentiation and neutrophil-specific programming. Cell Reports, 29, 2505–2519

Jaishy, B., Abel, E.D., 2016. Lipids, lysosomes, and autophagy. Journal of Lipid Research, *57*, 1619–1635.

Jeong, H., Tombor, B., Albert, R., Oltvai, Z.N., Barábasi, A.-L., 2000. The large scale organization of metabolic networks. Nature 407, 651-654.

Jiang, B.H., Liu, L.Z., 2008. Role of mTOR in anticancer drug resistance: perspectives for improved drug treatment. Drug Resist. Updates 11, 63-76.

Jimeno-Romero, A., Oron, M., Cajaraville, M.P., Soto, M., Marigomez, I., 2016. Nanoparticle size and combined toxicity of TiO2 and DSLS (surfactant) contribute to lysosomal responses in digestive cells of mussels exposed to TiO2 nanoparticles. Nanotoxicology, 10, 1168–1176.

Juste, Y.R., Cuervo, A.M., 2019. Analysis of Chaperone-Mediated Autophagy. Methods Mol. Biol., 1880, 703-727. doi:10.1007/978-1-4939-8873-0_47

Katsifis, S.P., Kinney, P.L., Hosselet, S., Burns, F.J., Christie, N.T., 1996. Interaction of nickel with 537 mutagens in the induction of sister chromatid exchanges in human lymphocytes. Mutat. Res., 359, 7-15.

Kirchin, M.A., Moore, M.N., Dean, R.T. and Winston, G.W., 1992. The role of oxyradicals in

intracellular proteolysis and toxicity in mussels. Mar. Environ. Res., 34, 315-320.

Koehler, A., Marx, U., Broeg, K., Bahns, S., Bressling, J., 2008. Effects of nanoparticles in *Mytilus edulis* gills and hepatopancreas - a new threat to marine life? Mar. Environ. Res., 66, 12–14.

Kurz, T., Terman, A., Gustafsson, B., Brunk, U.T., 2008. Lysosomes in iron metabolism, ageing and apoptosis. Histochemistry & Cell Biology, 29, 389-406.

Lee, D., Hong, J.H., 2020. Nanoparticle-mediated therapeutic application for modulation of lysosomal ion channels and functions. Pharmaceutics, 12, 217; doi:10.3390/ pharmaceutics12030217.

Lee, C.M., Huang, S.T., Huang, S.H., et al., 2011. C_{60} fullerene-pentoxifylline dyad nanoparticles enhance autophagy to avoid cytotoxic effects caused by the β-amyloid peptide. Nanomedicine, 7(1), 107-114.

Levine B (2005) Eating oneself and uninvited guests: autophagy-related pathways in cellular defense. Cell, 120, 159-162.

Lewis, A., Lipsitz, M.D., Ary, L., Goldberger, M.D., 1992. Loss of "complexity" and aging: potential applications of fractals and chaos theory to senescence. J. Amer. Med. Assoc. 267, 1806-1809.

Livingstone, D.R., Chipman, J.K., Lowe, D.M., Minier, C., Mitchelmore, C.L., Moore, M.N., Peters, L.D., Pipe, R.K., 2000. Development of biomarkers to detect the effects of organic pollution on aquatic invertebrates: recent molecular, genotoxic, cellular and immunological studies on the common mussel (*Mytilus edulis* L.) and other mytilids. Int. J. Environ. Pollut. 13, 56-91.

Lowe, D.M., 1988. Alterations in cellular structure of *Mytilus edulis* resulting from exposure to environmental contaminants under field and experimental conditions. Mar. Ecol. Prog. Ser. 46, 91-100

Lowe, D.M., Moore, M.N., 1979. The cytochemical distributions of zinc (Zn II) and iron (Fe III) in the common mussel, *Mytilus edulis*, and their relationship with lysosomes. *J.* mar. biol. Ass. U.K., 59, 851-858.

Lowe, D.M., Moore, M.N., Clarke, K.R., 1981. Effects of oil on digestive cells in mussels: quantitative alterations in cellular and lysosomal structure. Aquatic Toxicol., 1, 213-226.

Markovic, Z., Trajkovic, V. 2008. Biomedical potential of the reactive oxygen species generation and quenching by fullerenes (C_{60}). Biomaterials, 29, 3561–3573.

Minier, C., Moore, M.N., 1996a. Multixenobiotic resistance in mussel blood cells. Mar. Environ. Res. 42, 389-392.

Minier, C., Moore, M.N., 1996b. Rhodamine B accumulation and MXR protein expression in mussel blood cells: effects of exposure to vincristine. Mar. Ecol. Prog. Ser. 142, 165-173.

Mochida, K., Oikawa, Y., Kimura, Y., Kirisako, H., Hirano, H., Ohsumi, Y., Nakatogawa, H., 2015. Receptor-mediated selective autophagy degrades the endoplasmic reticulum and the nucleus. Nature 522, 59-362.

Moore, M.N., 1988. Cytochemical responses of the lysosomal system and NADPH-ferrihemoprotein reductase in molluscs to environmental and experimental exposure to xenobiotics. Mar. Ecol. Prog. Ser., 46, 81-89.

Moore, M.N., 2010. Is toxicological pathology characterised by a loss of system complexity? Mar. Environ. Res. 69, S37-S41.

Moore, M.N., 2020. Lysosomes, autophagy and hormesis in cell physiology, pathology and age-related disease. Dose Response, 2020; DOI: 10.1177/1559325820934227.

Moore, M.N., Allen, J.I. & McVeigh, A., 2006. Environmental prognostics: an integrated model supporting lysosomal stress responses as predictive biomarkers of animal health status. Mar. Environ. Res., 61, 278–304

Moore, M.N., Depledge, M.H., Readman, J.W., Leonard, P., 2004. An integrated biomarker-based strategy for ecotoxicological evaluation of risk in environmental management. Mutation Res., 552, 247-268.

Moore, M.N., Koehler, A., Lowe, D. & Viarengo, A., 2008. Lysosomes and autophagy in aquatic animals. In: Methods in Enzymology (D.Klionsky, Ed), 451, 582-620. Academic Press/Elsevier, Burlington.

Moore, M.N., Readman, J.A., Readman, J.W., Lowe, D.M., Frickers, P.E., Beesley, A., 2009. Lysosomal cytotoxicity of carbon nanoparticles in cells of the molluscan immune system: an *in vitro* study. Nanotoxicology, 3, 40-45.

Moore, M.N., Shaw, J.P., Ferrar Adams, D.R., Viarengo, A., 2015. Anti-oxidative cellular protection effect of fasting-induced autophagy as a mechanism for hormesis. Mar. Environ. Res. 107, 35-

44.

Moore, M.N., Shaw, J.P., Pascoe, C., Beesley, A., Viarengo, A., Lowe, D.M., 2020. Anti-oxidative hormetic effects of cellular autophagy induced by nutrient deprivation in a molluscan animal model. Marine Environmental Research, 156, 104903; https://doi.org/10.1016/j.marenvres.2020.104903.

Moore, M.N., Viarengo, A., Donkin, P., Hawkins, A.J.S., 2007. Autophagic and lysosomal reactions to stress in the hepatopancreas of blue mussels. Aquatic Toxicol., 84, 80-91.

Moore, M.N., Viarengo, A.G., Somerfield, P.J., Sforzini, S., 2013. Linking lysosomal biomarkers and ecotoxicological effects at higher biological levels. In - Ecological Biomarkers: Indicators of Ecotoxicological Effects, (Eds.C. Amiard-Triquet, J.C. Amiard, P.S. Rainbow), pp. 107-130. CRC Press, Boca Raton (Florida), New York & Oxford

Nakamura, S., Yoshimori, T., 2017. New insights into autophagosome-lysosome fusion. J. Cell Sci.,130(7), 1209-1216.

Oh, N., Park, J.H., 2014. Endocytosis and exocytosis of nanoparticles in mammalian cells. Int. J. Nanomedicine, 6;9 Suppl 1(Suppl 1):51-63. doi: 10.2147/IJN.S26592. PMID: 24872703; PMCID: PMC4024976.

Plant, A.L., Benson, D.M., Smith, L.C., 1985. Cellular uptake and intracellular localization of benzo(a)pyrene by digital fluorescence imaging microscopy. J. Cell Biol., 100, 1295-1308.

Rashid, F., Horobin, R.W., Williams, M.A., 1991. Predicting the behaviour and selectivity of fluorescent probes for lysosomes and related structures by means of structure-activity models. Histochem. J., 23, 450-459.

Reeves JF, Davies, S.J., Dodd N.J.F., Jha, A.N., 2008. Hydroxyl radicals (˙OH) are associated with titanium dioxide (TiO_2) nanoparticle-induced cytotoxicity and oxidative DNA damage in fish cells. Mutation Research (*Fundamental and Molecular Mechanisms of Mutagenesis*), 640, 113-122.

Rondags, A., Yuen, W.Y., Jonkman, M.F., Horváth, B., 2017. Fullerene C_{60} with cytoprotective and cytotoxic potential: prospects as a novel treatment agent in Dermatology? Exp. Dermatol., 26, 220-224.

Sanchís, J., Aminot, Y., Abad, E., Jha, A.N., Readman, J.W., Farré, M., 2018. Transformation of C_{60} fullerene aggregates suspended and weathered under realistic environmental conditions. Carbon, 128, 54–62.

Sayes, C.M., Fortner, J.D., Guo, W., Lyon, D., Boyd, A.M., Ausman, K.D., Tao, Y.J., Sitharaman, B., Wilson,L.J., Hughes, J.B., West, J.L., Colvin, V.L., 2004. The differential cytotoxicity of water-soluble fullerenes. Nano Letters, 4, 1881-1887.

Schlesinger, R.B., Zelikoff, J.T., Chen, L.C., Kinney, P.L., 1992. Assessment of toxicologic interactions resultingf rom acute inhalation exposure to sulfuric acid and ozone mixtures. Toxicol. Appl. Pharmacol., 115, 183-190.

Sedivy, R., 1999. Chaodynamic loss of complexity and self-similarity cancer. Med. Hypotheses 52, 271-274.

Seo, S.U., Woo, S.M., Kim, S.H., Min, K.-J. & Kwon, T.K., 2018. mTORC1/2 inhibitor and curcumin induce apoptosis through lysosomeal membrane permeabilization-mediated autophagy. Oncogene, 37, 5205-5220

Seranova, E., Connolly, K.L., Zatyka, M., Rosenstock, T.R., Barrett, T., Tuxworth, R.I., Sarkar, S., 2017. Dysregulation of autophagy as a common mechanism in lysosomal storage diseases. Essays Biochem., 61, 733-745.

Sforzini, S., Moore, M.N., Boeri, M., Bencivenga, M., Viarengo, A., 2015. Effects of PAHs and dioxins on the earth vorm *Eisenia andrei*: a multivariate approach for biomarker interpretation. Environ. Pollut., 196. 60-71.

Sforzini, S., Moore, M.N., Oliveri, C., Volta, A., Jha, A., Banni, M., Viarengo, A., 2018. Role of mTOR in autophagic and lysosomal reactions to environmental stressors in molluscs. Aquatic Toxicol., 195, 114–128.

Sforzini, S., Oliveri, C., Barranger, A., Jha, A.N., Banni, M., Moore, M.N., Viarengo, A., 2020. Effects of fullerene C_{60} in blue mussels: role of mTOR in autophagy related cellular/tissue alterations. Chemosphere, DOI: 10.1016/j.chemosphere. 2019.125707

Shannon, P., Markiel, A., Ozier, O., Baliga, N.S., Wang, J.T., Ramage, D., Amin, N., Schwikowski, B., Ideker, T., 2003. Cytoscape: a software environment for integrated models of biomolecular

interaction networks. Genome Res. 13, 2498-2504.

Shaw, J.P., Dondero, F., Moore, M.N., Negri, A., Dagnino, A., Readman, J.W., Lowe, D.M., Frickers, P.E., Beesley, A., Thain, J.E., Viarengo, A., 2011. Integration of biochemical, histochemical and toxicogenomic indices for the assessment of health status of mussels from the Tamar Estuary, U.K. Mar. Environ. Res., 72, 13-24.

Shaw, J.P., Moore, M.N., Readman, J.W., Mou, Z., Langston, W.J., Lowe, D.M., Frickers, P.E., Al-Moosawi, L., Pascoe, C., Beesley, A., 2019. Oxidative stress, lysosomal damage damage and dysfunctional autophagy in molluscan hepatopancreas (digestive gland) induced by chemical contaminants. Mar. Environ. Res., 152, 104825. doi.org/10.1016/j.marenvres.2019.104825.

Stelling, J., Sauer, U., Szallasi, Z., Doyle, F.J., Doyle, J., 2004. Robustness of cellular functions. Cell, 118, 675-685.

Stern, S.T., Adiseshaiah, P.P., Crist, R.M., 2012. Autophagy and lysosomal dysfunction as emerging mechanisms of nanomaterial toxicity. Particle and Fibre Toxicology, 9:20. https://doi.org/10.1186/1743-8977-9-20

Stone V., Donaldson, K., 2006. Nanotoxicology: signs of stress. Nature Nanotechnology, 1(1), 23–24.

Von Moos, N., Burkhardt-Holm, P., Köhler, A., 2012. Uptake and effects of microplastics on cells and tissue of the blue mussel *Mytilus edulis* L. after an experimental exposure. Environ. Science Technol., 46, 11327–11335.

Wang, F., Gómes-Sintes, R., Boya, P., 2018. Lysosomal membrane permeabilization and cell death. Traffic, 19, 918-931.

Ward, D. M., Leslie, J. D., & Kaplan, J., 1997. Homotypic lysosome fusion in macrophages: analysis using an in vitro assay. J. Cell Biol., 139(3), 665–673.

Winston, G.W., Moore, M.N., Straatsburg, I., Kirchin, M., 1991. Lysosomal stability in *Mytilus edulis* L.: potential as a biomarker of oxidative stress related to environmental contamination. Arch. Environ. Contam. Toxicol., 21, 401-408.

Yang, Y., Liu, X., Zhang, X.X., Korenaga, T., 2001. Study on the dynamic complexation between

protein and PAHs by capillary electrophoresis. Analyt. Sciences, 2001 17(ICAS2001): i1345-i1349.

Yu, Z., Persson, H.L., Eaton, J.W., Brunk, U.T., 2003. Intralysosomal iron: a major determinant of oxidant-induced cell death. Free Radical Biol. Med., 34(10), 1243-1252. doi:10.1016/s0891-5849(03)00109-6

Zanger, R.C., Davydov, D., Venna, S., 2004. Mechanisms that regulate production of reactive oxygen species by cytochrome P450. Toxicol. Appl. Pharmacol., 199, 316-31.

Zhang, S., Zhang, J., Chen, H., Wang, A., Liu, Y., Hou, H., Hu, Q., 2019. Combined cytotoxicity of co-exposure to aldehyde mixtures on human bronchial epithelial BEAS-2B cells. Environ. Pollut., 250, 250-261.

Zhao, Y.G., Zhang, H., 2019. Autophagosome maturation: an epic journey from the ER to lysosomes. J. Cell Biol., 218(3), 757-770.

Zhao, Y., Hu, X., Liu, Y., Dong, S., Wen, Z., He, W., Zhang, S., Huang, Q., Shi, M., 2017. ROS signaling under metabolic stress: cross-talk between AMPK and AKT pathway. Molecular Cancer (2017) 16:79. DOI 10.1186/s12943-017-0648-1.

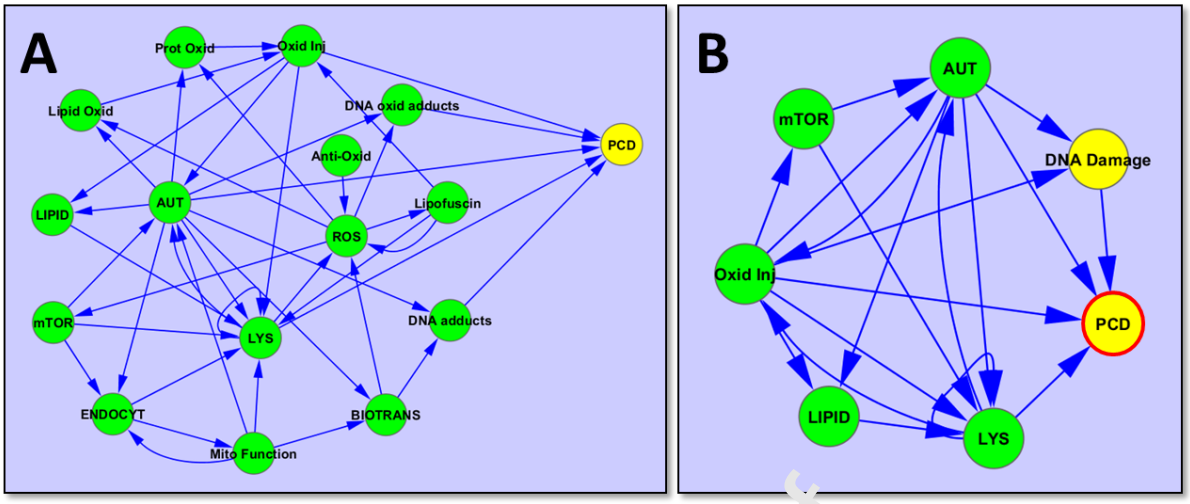

Fig. 1. **A.** Interaction network model based on the physiological and pathological processes represented by the biomarker investigations in mussel digestive cells. Processes represented include endocytosis (cell feeding), lysosomal function (highly connected hub), autophagy (highly connected hub), phosphorylated mTORC1 signalling, lysosomal lipid accumulation, oxidative cell injury, DNA damage, cytochrome P450 mediated biotransformation and Programmed Cell Death (PCD – yellow node:- apoptosis – type 1 PCD; autophagic – type 2 PCD; necrotic – type 3 PCD). **B.** Abbreviated network corresponding to the biomarkers actually deployed in the current study. The calculation of connectance % did not include values for yellow nodes DNA damage and PCD (red outline). Green nodes represent those included in the determination of system complexity (connectance - C_v%). AUT – autophagy, Anti-Oxid – anti-oxidative protection, BIOTRANS – Cytochrome P450 (CYP) mediated biotransformation, ENDOCYT – endocytosis, DNA adducts – organic xenobiotic derived adducts, DNA oxid adducts – oxidative adducts, LIPID – lysosomal triglyceride (lipidosis), Lipid Oxid – lipid peroxidation, Lipofuscin – ceroid lipofuscin (stress pigment), LYS – lysosomal function, mTOR – mTORC1, Mito Function – mitochondrial energy metabolism, Oxid Inj – oxidative cell injury, PCD – programmed cell death (apoptotic, autophagic and necrotic cell death), Prot Oxid – protein oxidation (carbonyls); and ROS – reactive oxygen species.

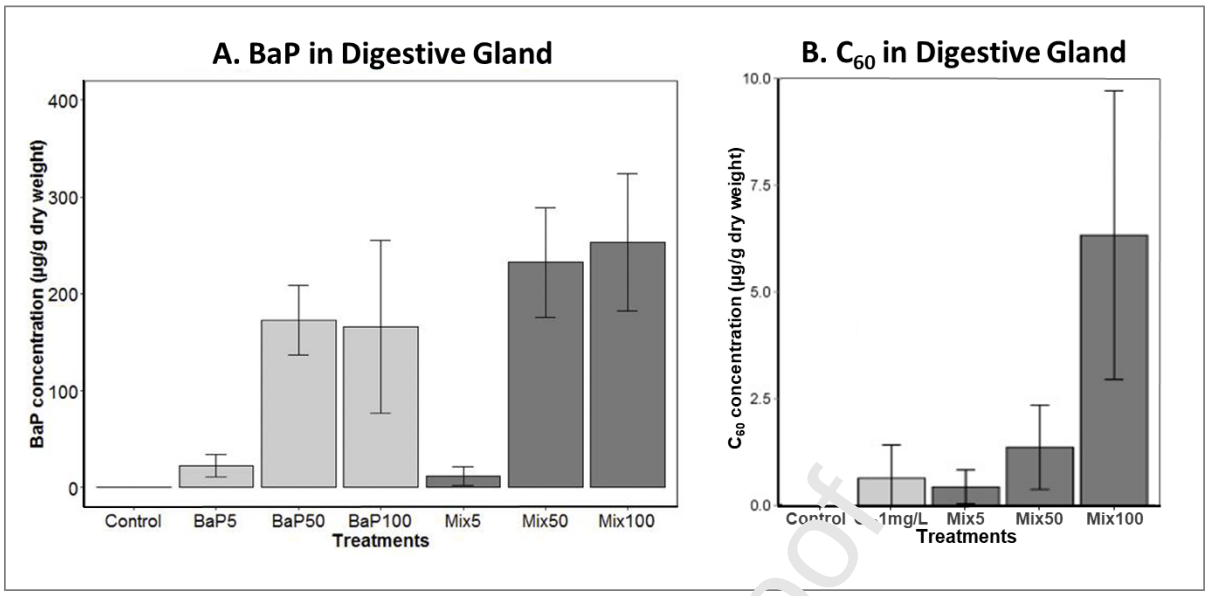

Fig. 2. C_{60} and BaP concentrations in digestive gland tissue.- A. gas chromatography-mass spectrometry (GC–MS) analyses of BaP in digestive gland (mean ± SE); B. liquid chromatography-mass spectrometry (LC–MS) analyses of C_{60} in digestive gland (mean ± SE)with C60 levels for Mix 100 treatment being significantly different from the controls and other treatments ($P \leq 0.05$, n = 3, Tukey post-hoc test) . Data adapted from Barranger et al. (2019a).

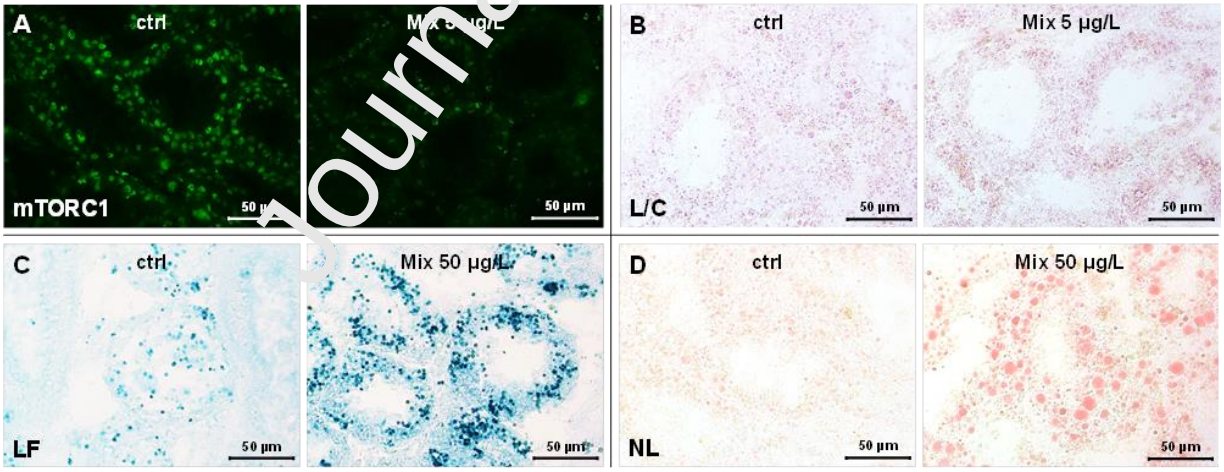

Fig. 3. Representative paired images of the lysosomal and autophagy-related biomarker changes in the digestive gland tissue sections from controls and exposed mussels: **A.** anti-phosphorylated-mTORC1 immunocytochemical fluorescence reaction (green: Chromeo conjugated secondary antibody); **B.** L/C volume ratio; **C.** lysosomal lipofuscin (LF) accumulation (lipofuscinosis);

and **D.** lysosomal lipid (NL) accumulation (lipidosis).

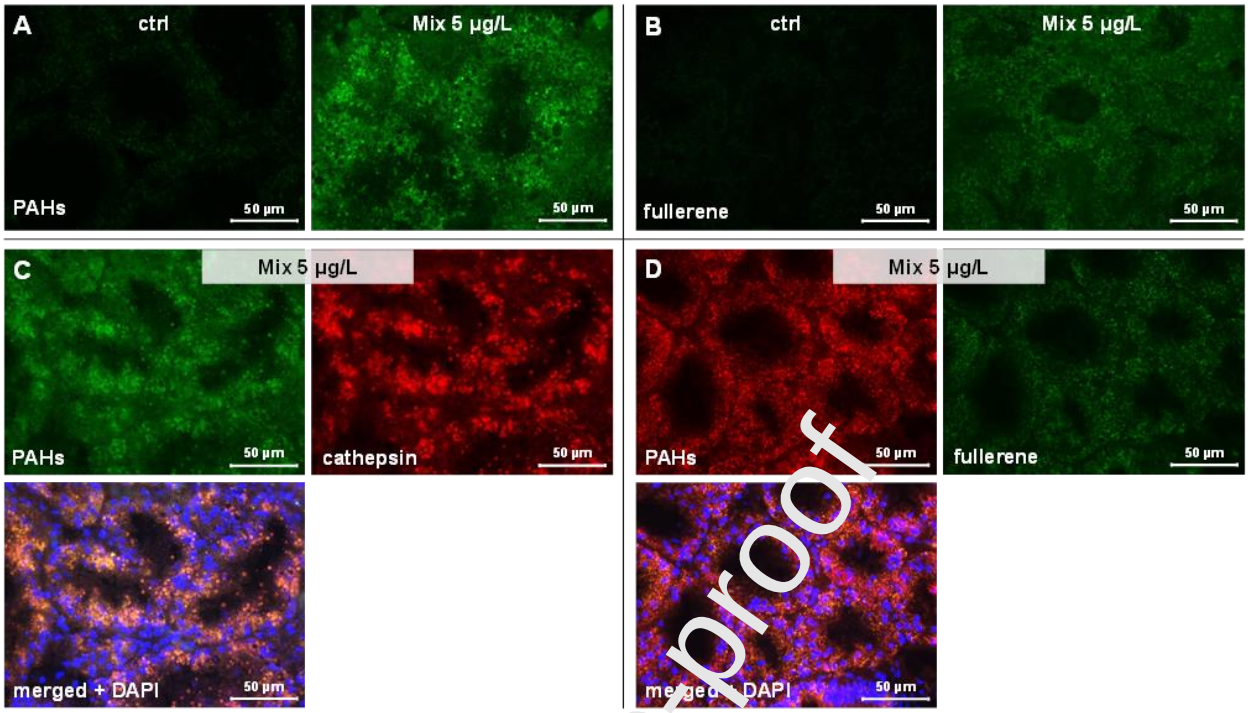

Fig. 4. **A.** Anti-PAHs immunofluorescence for the detection of BaP; **B.** anti-fullerene immunofluorescence (green: FITC conjugated secondary antibody) of digestive gland tissue sections from control and Mix 5 µg/L treated animals; **C.** double immunocytochemical fluorescent reactions in digestive cells from mussels treated with Mix 5 µg/L reacted with anti-PAHs and anti-cathepsin D antibodies (separate colour images for PAHs [FITC, green] and cathepsin D [DyLight 594, red]) - immunoreactivities were merged into a composite image, whereby the co-localization of both antigens resulted in a yellow colour; and **D.** double immunofluorescence of digestive cells from animals treated with Mix 5 µg/L reacted with anti-PAHs and anti-fullerene antibodies (separate colour images for PAHs [Alexa Fluor® 568, red] and fullerene [FITC, green] - immunoreactivities were merged into a composite image, whereby the co-localization of both antigens resulted in a yellow-orange colour. In the merged pictures, nuclei were stained with DAPI (blue fluorescence).

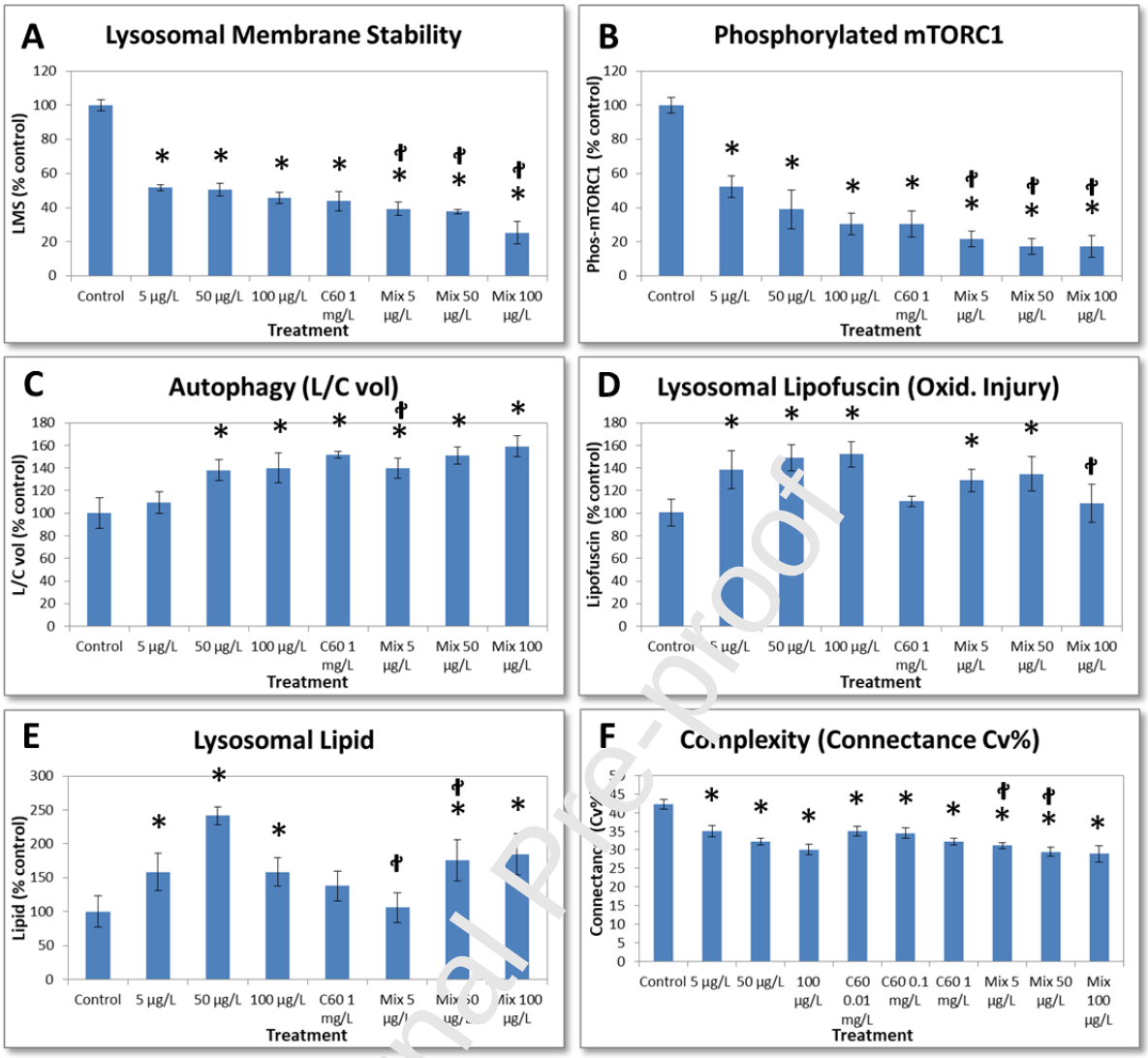

Fig. 5. Biomarker data for the experimental treatments with C_{60} fullerene (1 mg/L), BaP (5, 50 & 100 µg/L) and mixtures of both compounds: **A.** Lysosomal membrane stability (LMS); **B.** Lysosomal lipid (lipidosis); **C.** Autophagy measured as lysosomal volume / cell volume (L/C vol ratio); **D.** Phosphorylated mTORC1; **E.** Lipofuscin (lipofuscinosis); and **F.** Network complexity measured as **c**onnectance (C_v%) including 0.01 and 0.1 mg/L C_{60} fullerene (biomarker data from Sforzini et al., 2020). All treatments were tested against the control (***** $P \leq 0.05$; Mann-Whitney U test and t-test); and the biomarker and connectance values (mean ± 95% CL/√2, n = 5) are also significantly different ($P \leq 0.05$, t-test) if the error bars do not overlap (Lowe et al., 1981; Buzatto et al., 2015); □ $P \leq 0.05$ (t-test) for pairwise tests between BaP 5, 50 & 100 µg/L and MIX 5, 50 & 100 µg/L.

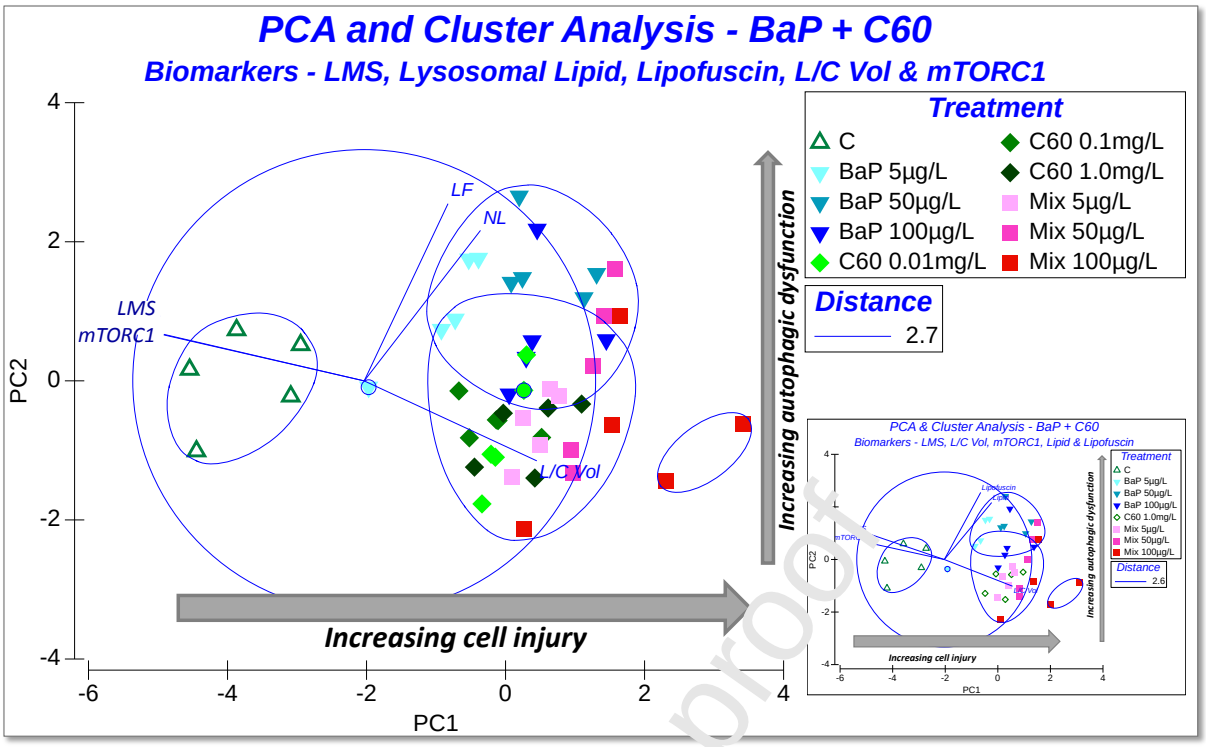

Fig. 6. Principal component (PCA) and cluster analysis of the C_{60} and BaP biomarker data biomarker data not including DNA damage, but including data for 0.01 and 0.1 mg/L C_{60}. Vectors indicate the directionality of specific biomarkers. **Arrows indicate:-** a. Increasing Cell Injury corresponding to the first principal component (PC1); and b. Increasing trend for Autophagic Dysfunction based on elevated intralysosomal lipofuscin and lipid, and corresponding to the second principal component (PC2). **Inset:-** PCA excluding data for 0.01 and 0.1 mg/L C_{60}. **Vectors:-** LMS – lysosomal membrane stability; L/C Vol – lysosome/cell volume ratio (autophagy biomarker); LF – lysosomal lipofuscin (lipofuscinosis); NL – lysosomal lipid (lipidosis); and mTORC1 – phosphorylated mTORC1.

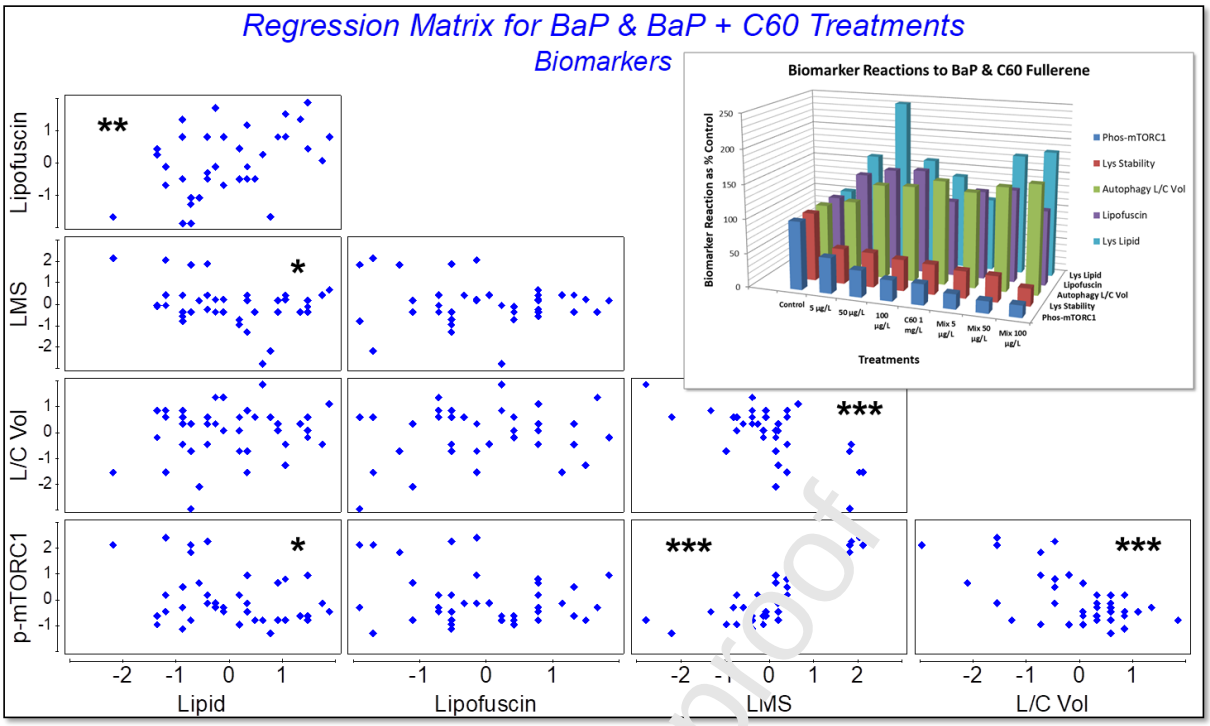

Fig. 7. Regression matrix for the C_{60} and BaP biomarker data. **Inset:-** 3D summary plot of the biomarker reactions to the experimental treatments. Pearson's correlation coefficient: * indicates $P \leq 0.05$; ** indicates $P < 0.01$; *** indicates $P \leq 0.001$; n = 40.

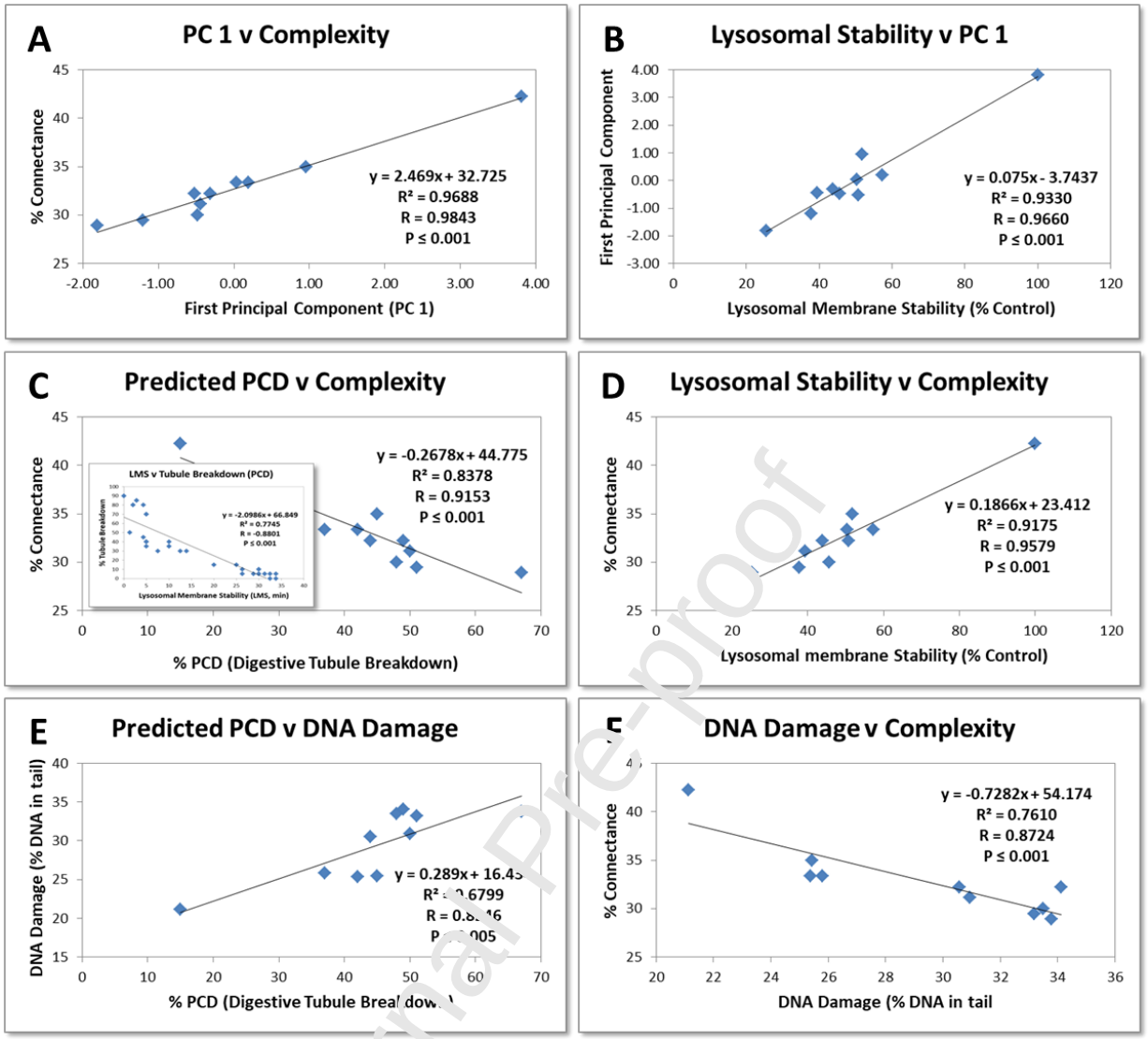

Fig. 8. Statistical modelling of system complexity (C_v%), lysosomal stability, predicted programmed cell death and DNA damage based on C_{60} and BaP biomarker data (including data for 0.01 and 0.1 mg/L C_{60}) versus: **A.** first principal component (PC 1) v complexity; **B.** Lysosomal membrane stability (LMS) versus PC 1; DNA damage (Comet); **C.** Predicted programmed cell death (PCD) v complexity (**Inset: –** LMS v digestive tubule breakdown as indicator of PCD); **D.** lysosomal stability versus complexity; and **E.** Predicted programmed cell death (PCD) versus DNA damage; and **F.** DNA damage versus complexity. Coefficient of determination (R^2), Pearson's correlation coefficient (R), and probability values (one-tailed test).

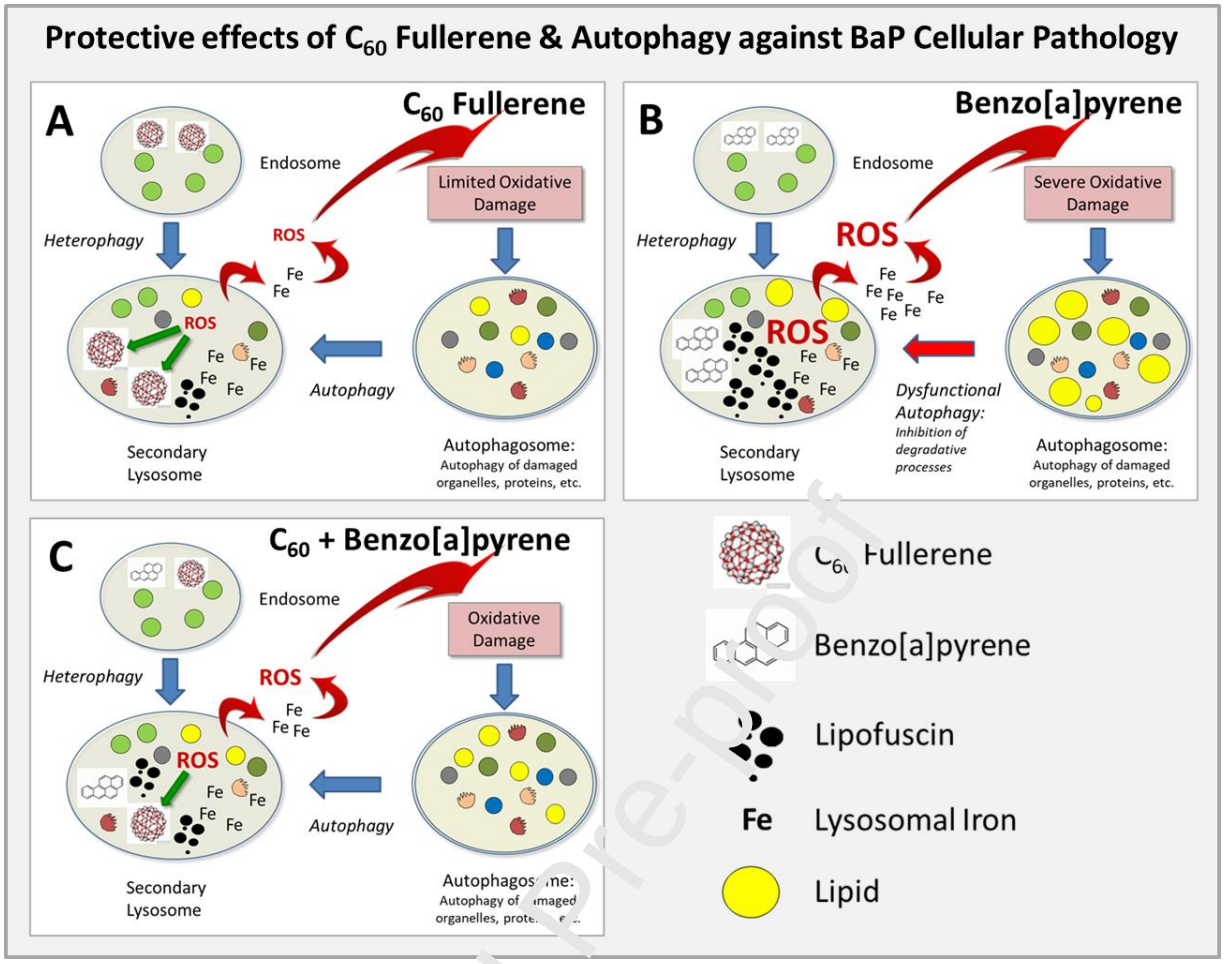

Fig. 9. Subcellular reactions to:- **A.** C_{60} fullerene; **B.** BaP; and **C.** C_{60} + BaP. Conceptual model deduced from the observed lysosomal cytoprotective effects of C_{60} scavenging (green arrows) of intra-lysosomal ROS (generated by iron and lipofuscin-bound iron) and autophagic cytoprotection against BaP induced oxidative cell injury (i.e., autophagic dysfunction, oxidative stress and including DNA damage). Intralysosomal iron is released when lysosomal membrane stability is reduced by accumulation of C_{60} and BaP, as well as the injurious action of lysosomal hydrolases and ROS (i.e., increased lysosomal membrane permeability; Kurz et al., 2008; Stern et al., 2012; Yu et al., 2003). Increased autophagy of lipid results in lipidosis that tends to inhibit lysosomal degradative processes contributing to autophagic and lysosomal dysfunction.

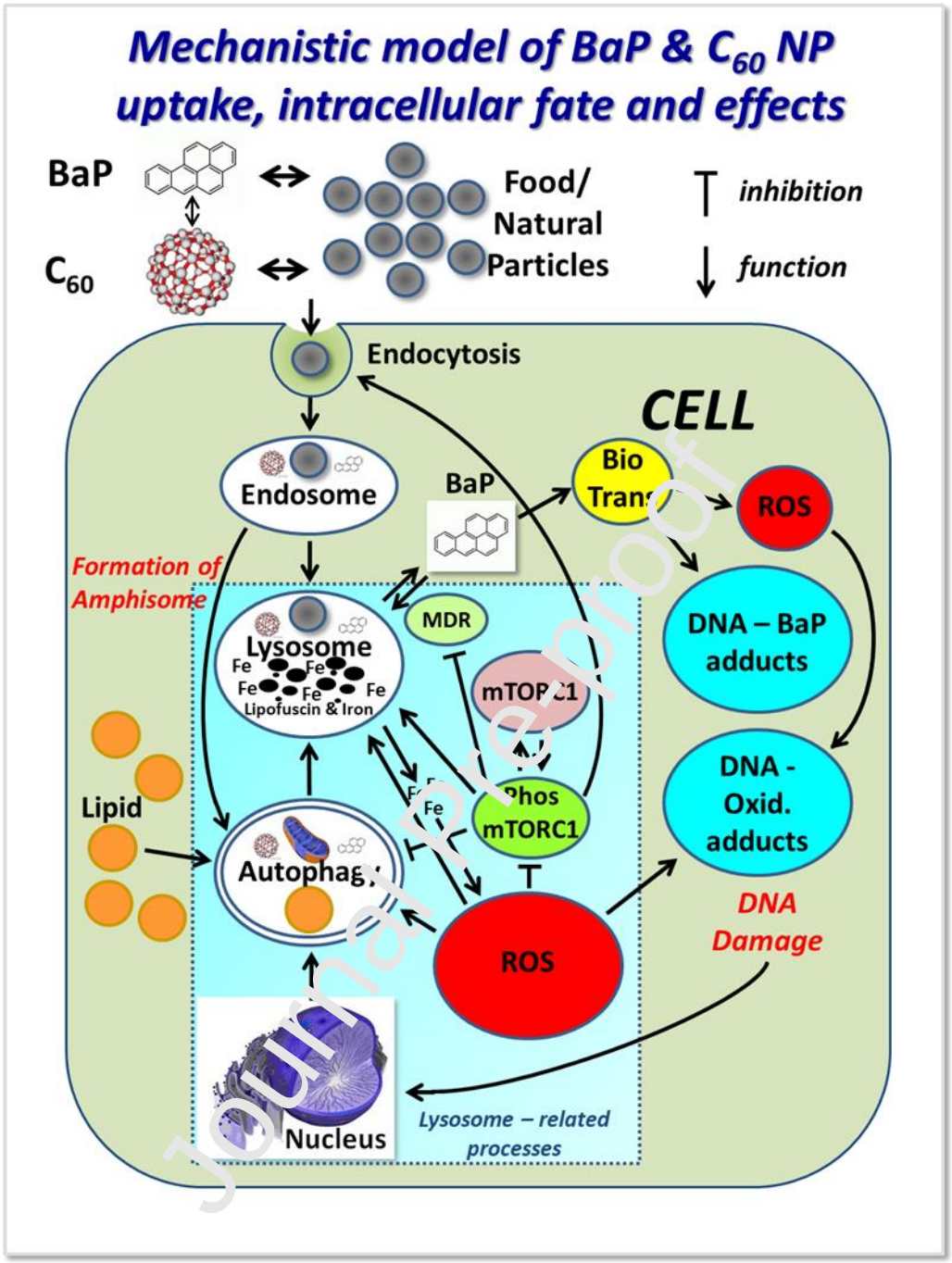

Fig. 10. Diagrammatic representation of an explanatory mechanistic framework for the interconnected cellular reactions to C_{60} and B*a*P based on the biomarker data, network modelling and other published sources in the scientific literature (Sforzini et al., 2018). Destabilisation of the lysosomal membrane (i.e., increased permeability) induced by overload of BaP and C_{60} will cause lysosomal hydrolase and iron (Fe) release into the cytosol with resultant generation of reactive oxygen species (ROS) and degradation of macromolecules. Autophagy will have a

cytoprotective effect by transporting oxidatively damaged proteins, damaged organelles (e.g., mitochondria) and damaged genomic components into the lysosomal compartment. Autophagosomes can also fuse with late endosomes to form amphisomes, which then mature into secondary lysosomes (Nakamura & Yoshimura, 2017). ROS will inhibit phosphorylated mTORC1 (active form), which will induce augmented autophagy (Brunk & Terman, 2002; Chen et al., 2010; Moore et al., 2006, 2015; Sforzini et al., 2018, 2019). Inhibition of mTORC1 will also inhibit endocytosis, further reduce lysosomal membrane stability and activate Pgp40 (Boya, 2012; Flinn & Backer, 2010; Jiang & Liu, 2008). The increased flux of ROS will also contribute to fatty change (steatosis), with accumulation of autophagocytosed lipid within the lysosomal compartment resulting in lysosomal and autophagic dysfunction. Increased ROS flux will also cause oxidative damage to DNA (Canova et al., 1998); and enhanced autophagy may engulf portions of damaged and undamaged genomic material through partial nuclear autophagy (Buckland-Nicks & Hodgson, 2003; Mochida et al., 2015). Autophagy of nuclear DNA may contribute to autophagic and/or apoptotic programmed cell death as a pathological endpoint (Lowe, 1988; Lowe et al., 1981). ROS - reactive oxygen species; Phos mTOR - active phosphorylated form of mTORC1 cell signalling system; mTOR - inactive dephosphorylated form of mTORC1; MDR - Pgp40 multidrug transporter; Biotrans Ph I & II - Phase I and II biotransformation system (Canova et al., 1998).

Table 1. Pearson's correlation coefficients for correlations between the first and second principal components (PC1 & PC2) and individual biomarkers.

Principal Components	***Lysosomal Lipid (Lipid)***	***Lipofuscin***	***Lysosomal Stability (LMS)***	***Lys/Cell Volume (L/C Vol)***	***mTORC1 (phosphorylated)***
PC1	-0.5413	-0.4160*	0.8739***	-0.7799***	0.8874***
PC2	0.6509***	0.7663***	0.2973	-0.3048	0.1955

PC1 represents 52.5% of the variability, and PC2 24.6 % of the variability. * Indicates significance at the 5%

level, ** significance at the 1% level, and *** significance at the 0.1% level, two-tailed test; n = 40. Does not include the data for 0.01and 0.1 mg/L C_{60}.

Table 2. Intracellular interactions (edges or links E) used in the network model***** for the determination of connectance (Cv %) as a measure of system complexity.

Interaction	**Abbreviation**	**Biomarker**
Lysosomal function & Autophagy	LYS-AUT	Lysosomal membrane stability (LMS)
Lysosomal function & Oxidative injury	LYS-Oxid Inj	Lysosomal membrane stability (LMS)
Autophagy & Lysosomal function	AUT-LYS	Lysosome/Cell volume ratio (L/C vol)
Autophagy & Oxidative injury	AUT-Oxid Inj	Lysosome/Cell volume ratio (L/C vol)
Autophagy & DNA damage	AUT-DNA damage	Lysosome/Cell volume ratio (L/C vol)
Triglyceride lipid & Lysosomal function	LIPID-LYS	Lysosomal lipid (triglyceride)
Triglyceride lipid & Autophagy	LIPID-AUT	Lysosomal lipid (triglyceride)
Phosphorylated mTORC1 & Lysosomal function (permeability)	mTOR-LYS	Phosphorylated mTORC1 kinase (phos-mTORC1)
Phosphorylated mTORC1 & Autophagy	mTOR-AUT	Phosphorylated mTORC1 kinase (phos-mTORC1)
Oxidative cell injury & Autophagy	Oxid Inj-AUT	Lysosomal Lipofuscin
Oxidative cell injury & Lysosomal function	Oxid Inj-LYS	Lysosomal Lipofuscin
Oxidative cell injury & Lipid (fatty change)	Oxid Inj-LIPID	Lysosomal Lipofuscin
Oxidative cell injury & phosphorylated mTORC1	Oxid Inj-mTOR	Lysosomal Lipofuscin
Oxidative cell injury & DNA damage	Oxid Inj-DNA damage	Lysosomal Lipofuscin

***** PCD node (vertex) was not included in the determination of complexity in the network (Fig. 1B).

Table 3. Interaction Factors (IF) for the combined effects of C_{60} fullerene and benzo[a]pyrene (BaP) on the various biomarkers and connectance (C_v%).

Treatment Mixture	***DNA Damage (COMET)***	***Lysosomal Stability (LMS)***	***mTORC1 (phos-mTORC1)***	***Lysosomal Lipid***	***Lysosomal Lipofuscin***	***Autophagy (Lysosomal/ Cell Volume Ratio)***	***Network Complexity (Connectance – C_v%)***
Mix C_{60} 1mg/l + BaP 5µg/l	-7.48 ± 6.63 (0 ± 6.31)	-44.0* ± 8.7 (0 ± 7.72)	-39.1* ± 13.2 (0 ± 11.74)	-90.4* ± 47.5 (0 ± 42.1)	-21.81 ± 23.34 (0 ± 21.00)	-21.9 ± 21.5 (0 ± 18.9)	-6.12* ± 2.42 (0 ± 2.30)
Mix C_{60} 1mg/l + BaP 50µg/l	-10.39□ ± 6.42 (0 ± 5.97)	-43.2* ± 8.7 (0 ± 8.58)	-47.9* ± 16.6 (0 ± 15.65)	-104.25* ± 46.1 (0 ± 34.6)	-25.77 ± 16.99 (0 ± 16.99)	-39.0□ ± 20.5 (0 ± 18.7)	-7.24* ± 2.37 (0 ± 2.05)
Mix C_{60} 1mg/l + BaP 100µg/l	-12.69 * ± 6.05 (0 ± 5.82)	-36.0* ± 11.0 (0 ± 8.28)	-56.6* ± 13.2 (0 ± 11.74)	-12.9 ± 48.4 (0 ± 37.7)	-54.71* ± 21.08 (0 ± 16.92)	-32.9□ ± 19.5 (0 ± 16.6)	-8.89* ± 3.13 (0 ± 1.98)

Interaction Factor ± 95% Confidence Limit / √2 (Buzatto et al., 2015). * indicates significance at the 5% level, and □ indicates significance at the 10% level. A negative IF indicates antagonism; an IF of 0 indicates additivity; and a positive IF indicates synergism. Statistical significance as indicated by * was determined by testing for overlap between the mixture IF ± 95% CL/√2 and the predicted additive value for C_{60} and BaP, assumed to have an IF = 0 ± 95% CL/√2, where the confidence limit is derived from the $SEM_{(add)}$ value for the additive C_{60} and BaP. DNA damage data was incorporated from Barranger et al. (2019a). Additive values (IF = 0 ± 95% CL/√2) are shown in parentheses for each treatment and biomarker.

Declaration of competing interests

☒ The authors declare that they have no known competing financial interests or personal relationships that could have appeared to influence the work reported in this paper.

☐The authors declare the following financial interests/personal relationships which may be considered as potential competing interests:

CREDIT Author Statement

Michael N. Moore 40%

Susanna Sforzini 20%

Aldo Viarengo 5%

Audrey Barranger 5%

Yann Aminot 5%

James W. Readman 5%

Andrei N. Khlobystov 5%

Volker M. Arlt 5%

Mohamed Banni 5%

Awadhesh N. Jha 5%

Graphical abstract

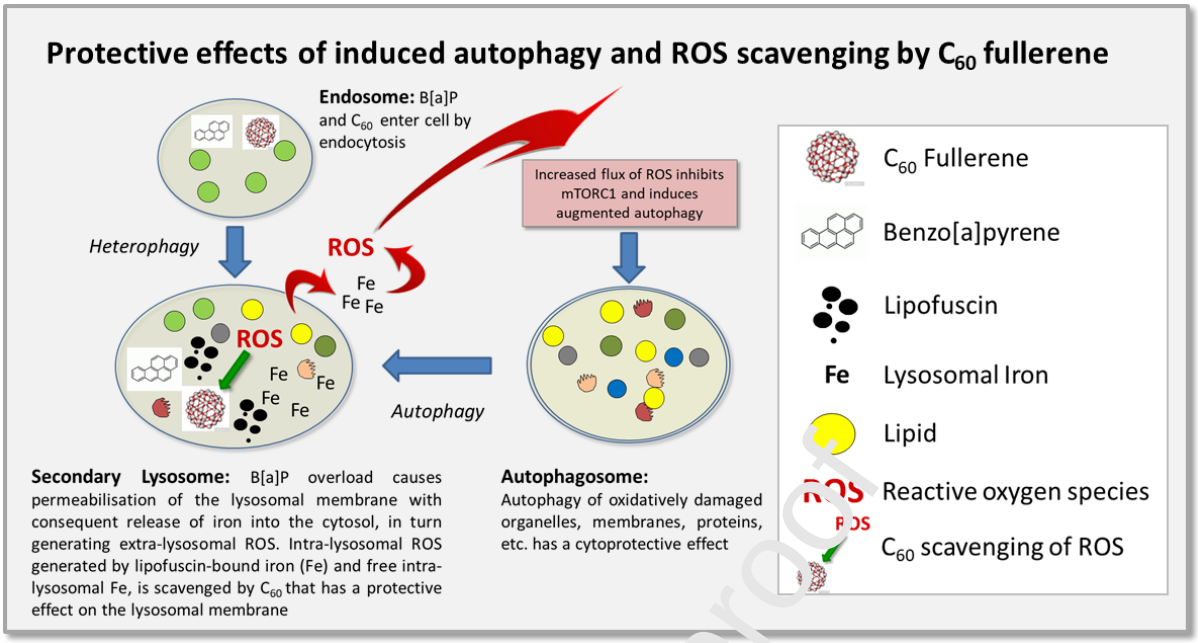

Highlights

- Simultaneous exposure to C_{60} fullerene (C_{60}) and benzo[a]pyrene (BaP) induced antagonistic subcellular interactions in the digestive cells of the digestive gland of the marine blue mussel.
- Both C_{60} and BaP were sequestered in the endolysosomal system where they induced adverse cellular pathological reactions including autophagy; however, those reactions induced by BaP were more severe, with evidence of dysfunctional autophagy.
- Both C_{60} and BaP caused lysosomal overload leading to lysosomal membrane destabilisation (i.e., increased lysosomal membrane permeability), resulting in probable iron release into the cytosol, where it generated harmful reactive oxygen species (ROS) that contributed to oxidative cell injury including DNA damage.
- Network (complexity) modelling of the molecular and subcellular pathology facilitated data interpretation and indicated that autophagy, together with intralysosomal scavenging of ROS by C_{60}, is having a cellular protective effect, compared to exposure to BaP alone.